Solutions to large beam-deflection problems by Taylor series and Padé approximant for compliant mechanisms

Ke Wu, Gang Zheng

Highlights

Solutions to Large Beam-deflection Problems by Taylor series and Padé approximant for Compliant Mechanisms

Ke Wu,Gang Zheng

- We solved large beam-deflection problems by Taylor series method.
- We solved large beam-deflection problems by Padé approximant.
- We provided convergence analysis on the 2 methods.
- We proved the feasibility of modeling CMs using the 2 methods.

Solutions to Large Beam-deflection Problems by Taylor series and Padé approximant for Compliant Mechanisms*

Ke Wu[a], Gang Zheng[a,*]

[a]Université de Lille, Inria, CNRS, Centrale Lille, UMR 9189 CRIStAL, Lille, F-59000, France

ARTICLE INFO

Keywords:
Compliant Mechanisms
Euler-Bernoulli Beam Theory
Boundary Value Problems (BVP)
Taylor Series
Padé approximant

Abstract

Compliant Mechanisms (CMs) serve as a promising alternative for transferring motion, force and energy compared to rigid mechanisms. The mentioned desired function is achieved by making the most of the elastic deflection of all built-in flexible members in CMs, such as slender straight beams and slender initially curved beams (ICBs). Therefore, accurately characterizing the deformation of these slender beams plays a considerable role in modeling CMs. As is well-known in the field of CMs, static planar large deflection of slender beams can be modeled via Euler Bernoulli beam theory, and it's essentially a boundary value problem (BVP). In this paper, we propose to use Taylor series method and Padé approximant to solve this BVP in a more efficient manner compared to the previous work. Its accuracy and efficiency have been compared with weighted residual method and also verified by solid-mechanics-based Finite Element Method (FEM) respectively. The feasibility of the proposed method has also been proved in terms of synthesizing CMs where three representative cases are studied.

1. Introduction

1.1. Compliant mechanisms

Compliant Mechanisms (CMs) have presented several desired properties in mechanical applications, gradually becoming a hot research area in recent years [1]. Different from rigid mechanisms, CMs demonstrate a new concept for energy (including force and motion) transferring that merely depends on the elastic deformation of the built-in flexible members [1][2]. This novel concept therefore enables CMs to present several more promising features than rigid ones [1][2], such as energy-saving actuation [1], simplified fabrication process [3], simple mechanical maintenance [2] and more precise motion under the same mechanism dimensions [4]. These mentioned advantages have been demonstrated in many CM-involved applications [1][3], for instance, MEMs [5], aircraft engineering [6], surgical applications [7], high-precision motion stage [4] and so on. In particular, Howell and his coworkers have done some impressive work on Origami mechanisms using CMs [8], which gradually becomes one of the hottest and newest areas in the academic field of CMs. Therefore, to properly design CMs, accurately and efficiently modeling slender beams is of great importance [9] where there are 2 major aspects: first, the **fundamental modeling theory** should be properly chosen; second, and the corresponding analytical or numerical **methods** that can implement the mentioned theories are highly needed.

1.2. The essence of modeling slender beams

As stated in the previous section, we would like to first stress and clarify that the **fundamental modeling theory** used for characterizing beam deflection and the corresponding **methods** to solve the derived governing equations are totally two different concepts. For example, beam theory is the theory used for characterizing the elastic behavior of slender beams while elliptical integral method [10] is just one method to solve the governing equations behind the theory. Similarly, the so-called Finite Element Method (FEM) used in this field essentially means using FEM to solve the governing equations behind solid mechanics or beam theory where solid mechanics or beam theory is the used theory and FEM is the computational method [11]. **Note that** seeking for effective theories and corresponding efficient methods to model flexible slender beams is always essential since they can significantly improve the accuracy and efficiency in topology model-based optimization of CMs [12] .

Therefore, in the following subsections, we mainly review and also recall the essence of Euler Bernoulli beam theory since it's the most commonly-dependent, simplest and straightforward theory in CMs. Likewise, the commonly-used methods to handle it will be briefly reviewed and discussed accordingly.

ORCID(s):

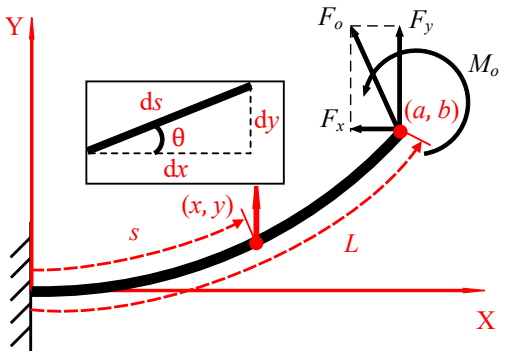

Figure 1: General loading beam-end loading of a slender beam

1.2.1. Euler Bernoulli beam theory

The famous Euler Bernoulli beam equation implies that the curvature $\frac{\mathrm{d}\theta}{\mathrm{d}s}(s)$ of the deflected slender beam at some point s, or equivalently point $(x(s), y(s))$ is proportional to the external moment $M(s)$ exerted at the same point s or equivalently point $(x(s), y(s))$:

$$EI\frac{\mathrm{d}\theta}{\mathrm{d}s} = M(s), \quad s \in [0, L] \tag{1}$$

where $\theta(s)$ refers to the rotation angle of the point s with respect to X axis as shown in Fig. 1; E is the Young's modulus of the material; I denotes the second moment of inertia of the cross-section area; L denotes the beam length; F_x, F_y and M_o are the *constant* forces and moment exerted at the beam-end point $s = L$. The graphical explanation is presented in Fig. 1.

Then, considering the varying cross-section along the beam axis and an initial curvature of the slender beam, we can arrive at:

$$\frac{\mathrm{d}\theta}{\mathrm{d}s} = \frac{M(s)}{EI(s)} + \frac{1}{R(s)} \tag{2}$$

where $I(s)$ denotes the second moment of inertia of the cross section area at point s, which implies the cross section may vary along the beam axis; similarly, $\frac{1}{R(s)}$ represents the initial curvature of the slender beam implying that the initial curvature may vary along the beam axis as well.

According to the definition of $M(s)$ in Eq. (1), $M(s)$ is the exerted moment at any arbitrary point s or equivalently $(x(s), y(s))$ on the beam due to all external loads on the beam. Therefore, $M(s)$ can be formulated as:

$$M(s) = F_y(x(L) - x(s)) + F_x(y(L) - y(s)) + M_o \tag{3}$$

Rearranging Eq. (2) and Eq. (3), we will end up with:

$$EI(s)\frac{\mathrm{d}\theta}{\mathrm{d}s} = F_y(x(L) - x(s)) + F_x(y(L) - y(s)) + M_o + \frac{EI(s)}{R(s)} \tag{4}$$

Differentiating (4) to eliminate the constant variables $x(L)$, $y(L)$ and M_o, we can obtain:

$$E\frac{\mathrm{d}I}{\mathrm{d}s}\frac{\mathrm{d}\theta}{\mathrm{d}s} + EI(s)\frac{\mathrm{d}^2\theta}{\mathrm{d}s^2} = -(F_y\cos\theta(s) + F_x\sin\theta(s)) + E\left(\frac{\frac{\mathrm{d}I}{\mathrm{d}s}(s)}{R(s)} - \frac{I(s)\frac{\mathrm{d}R}{\mathrm{d}s}(s)}{R(s)^2}\right) \tag{5}$$

where $\frac{\mathrm{d}x}{\mathrm{d}s} = \cos\theta$ and $\frac{\mathrm{d}y}{\mathrm{d}s} = \sin\theta$ are utilized. Note that (5) implies Euler Bernoulli beam theory can handle slender beams with varying cross sections and varying curvature along the beam axis, and there are many decent works regarding the aforementioned [9][13][14]. However, for standard manufacturing process in CMs, there exist many

contributions dealing with the following common cases, which are the simpler cases of (5): slender straight beams or initially curved beams (ICBs) with constant cross-section or constant initial curvature. Therefore, we can just narrow down the scope of the studied problem by simplifying (5):

$$\text{D.E. } EI\frac{\mathrm{d}^2\theta}{\mathrm{d}s^2} = -\left(F_y\cos\theta(s) + F_x\sin\theta(s)\right) \tag{6}$$

where $\frac{\mathrm{d}I}{\mathrm{d}s}(s) = 0$ and $\frac{\mathrm{d}R}{\mathrm{d}s}(s) = 0$ are used. Besides, 2 more boundary conditions are needed: $\theta(0) = 0$ implying that the tangent angle at $s = 0$ is zero since it is fixed; $\frac{\mathrm{d}\theta}{\mathrm{d}s}(L) = \frac{M_o}{EI} + \frac{1}{R}$ with $\frac{1}{R}$ being the constant initial curvature of the studied flexible beam (circularly curved beams) which is derived from Euler-Bernoulli beam equation at $s = L$. Therefore, we will end up with a boundary value problem (BVP) of ODE (6):

$$\begin{aligned}&\text{D.E. } \frac{\mathrm{d}^2\theta}{\mathrm{d}s^2} = -\frac{F_y}{EI}(\cos\theta(s) + \frac{F_x}{F_y}\sin\theta(s))\\ &\text{B.C. } \theta(0) = 0\\ &\qquad \frac{\mathrm{d}\theta}{\mathrm{d}s}(L) = \frac{M_o}{EI} + \frac{1}{R}\end{aligned} \tag{7}$$

where $\frac{1}{R} \to 0$ means the studied beam has no initial curvature (straight beam). Note that nearly all existing commonly used methods to handle beam-deflection problems are based on (7) [9][15], and these methods are briefly reviewed in the next section. For a more comprehensive review about modeling methods for large deflection of slender beams in CMs, [9] is recommended.

1.2.2. Commonly used modeling methods for large deflection of slender beams in CMs

To handle (7), CM researchers have found out many effective methods, which are mainly classified into 2 categories: analytical methods and numerical methods.

1. Analytical methods: elliptical integral method was introduced by Howell [1] to solve BVP (7). Theoretically, this method is the most accurate one since it's analytical. However, in practice, it is implemented in a semi-analytical manner since some complex integrals need to be numerically calculated.

   Remark 1. *Pseudo rigid body model (PRBM) [1], also proposed by Howell, essentially introduced a unique modeling concept where the deflection of a slender beam can be physically represented by that of a rigid mechanism. It serves as an effective modeling option at the early stage of design process. Note that it is definitely not the analytical solution to the original BVP (7) although it has a closed-form formulation.*

2. Numerical methods: BCM [16], proposed by Awtar, serves as an effective method of solving beam-deflection problems only within intermediate range where the curvature $\frac{\mathrm{d}\theta}{\mathrm{d}s}$ defined in (7) is linearized and rearranged as $\frac{\mathrm{d}^2y}{\mathrm{d}x^2}$ in a global frame for easier and more straightforward solution. Dr. Chen then extended this work and proposed Timoshenko Beam Constraint Model (TBCM) for the purpose of characterizing stubby beams (which takes the influence of shear force into account) [17]. To handle large-deflection problems, several chained algorithms are available: chained BCM [18] and chained PRBM [19–26] (see Remark 2 for details about chained-PRBM). Note that using chained algorithms to model CMs inevitably leads to high dimensional models, which is logically time-consuming to solve. FEM is often used to analyze large beam-deflection problems in CM research community. Essentially speaking, it's a method for numerically solving differential equations in engineering [11]. Therefore, FEM can handle the governing BVP (7) derived from Euler-Bernoulli beam theory, and it can also deal with the governing equations behind solid mechanics that describe beam deflection. However, FEM develops high-dimensional computational models, which may result in high computational expenses, for example, using solid mechanics to handle 3D modeling. In particular, using FEM to solve planar linear beam theories may still present desired efficiency in some cases [13][14]. This is why many CM researchers tend to use FEM-based commercial software (such as ANSYS, COMSOL and ABAQUS) only as a verification method but not quite a commonly used option for model-based optimization of CMs [9]. Mathematically speaking, (7)

is essentially a BVP of an ordinary differential equation (ODE) so weighted residual methods (denoted as WRM in this paper), finite difference method and shooting method [13][14] can therefore be utilized to approximate the solution of BVP (7) [15].

Remark 2. *Chained-PRBM artfully transforms the static beam deflection into a kinematic motion of a rigid mechanism where a limited number of rigid links associated with stiffness joints to approximate the solution of* (7)*. Basically, in the current literature, there are mainly two types of Chained-PRBM.*

(a) *The first type is the classic one where a small number of rigid links are used always with the need of estimating model parameters. For example, [1] provides a closed-form formulation for analyzing large deflection, which is significantly useful in the process of first-stage design. However, it suffers from the limitation of predicting larger end slope of flexible beams. The method proposed in [27] is also efficient since only one unknown needs to be solved (see Eq. 13 in [27]) using Newton's method or its relatives. However, it also needs to estimate the model parameters in advance. To us, this method is more like using a large number of loading cases to train the best parameters for the model via optimization (see Eq. 15 in [27]). This type of 'learning' strategies is common in the field of machine learning. Only if the number of training cases (loading cases) approach infinite, the final model will always converge to the correct or accepted solutions under given convergence criteria [28].*

(b) *[29] is another typical type. If the number n of the rigid links is large enough or approaches infinite, this Chained-PRBM can accurately approximate the solution of* (7) *essentially since:*

$$M(s) = K\delta\theta = \frac{EI}{l}\delta\theta \tag{8}$$

where l is the length of each rigid link and $l = \frac{L}{n}$ *with L being the beam length. If the number n approaches infinitely large, equivalently, l approaches infinitely small, we have*

$$M(s) = K\delta\theta = EI\lim_{l\to 0}\frac{\delta\theta}{l} = EI\frac{\mathrm{d}\theta}{\mathrm{d}s} \tag{9}$$

with the boundary conditions available. Then, this method directly goes back to numerically solve BVP (7) *with reliable accuracy. However, due to the large number of links discretized, it ends up with a large number of unknowns to be numerically solved. As a result, the group of equations derived from the principle of minimal potential energy or Euler equation (moment equilibrium) can be solved by Newton's method or its relatives. The high dimension of the Jacobian matrix may result in expensive computational cost when calculating its inverse [30].*

As summarized in the current literature, previous numerical frameworks, such as beam-theory-based chained-algorithms and solid-mechanics-based or beam-theory-based FEM, for characterizing the large deflection of slender beams need to solve a large number of unknowns [18][19], which can be regarded that they all aim to locally approximate the solution of BVP (7). To increase the accuracy of the results, we need to increase the number of discretization to a certain level, which however may result in more computational expenses. In the recently published work [15], the authors proposed to use several weighted residual methods to numerically solve Euler Bernoulli beam equation, which is essentially using a high-order polynomial with unknown coefficients to approximate the solution of BVP (7). In [15], 6th-order polynomials are used so still 7 unknowns need to be solved (although the number of unknowns has been reduced quite a lot). Normally, the unknowns that exist in a group of developed nonlinear equations are solved by Newton Raphson method and its relatives. In this process, the larger number of unknowns yields higher dimension of the Jacobian matrix and its inverse matrix, resulting in more computational expense [31]. Especially, when applying Newton-type method to seek optimal values of those multi-variables might yield local minima, depending on the chosen initial conditions, which is a well-known issue when applying such an approach. One solution to overcome this problem is to reduce the number of unknowns to be solved. Motivated by this idea, in this paper, we propose to use high-order Taylor series method and rational functions (Padé approximant) but with only 1 unknown to approximate the solution of BVP (7). In particular, we have noticed some inspiring works where Taylor series method and Padé approximant are used to handle the relatives of BVP (7) but only certain simpler cases are considered also without taking practical mechanical applications like CMs into account [32][33]. Roughly speaking, we first construct a high-order polynomial as the approximate solution of BVP (7) via Taylor expansion at $s = 0$. By using most of the information

of ODE (6), all coefficients of such an approximation can be then written as functions of only 1 unknown. Similarly, we can also construct a rational function to do so as well. Finally, the only unknown variable of the 2 constructed functions can be solved simply by satisfying the boundary conditions of (7). Compared to [32][33], this paper deals with more complex scenarios, such as varying curvature and varying cross sections, and also proves the feasibility of conducting mechanism synthesis for CMs using the proposed methods as well.

1.3. Main content of this paper

In this paper, we first present the derivation of using Taylor series method and rational functions (Padé approximant) to handle BVP (7) respectively. Then, the advantages and limitations of the 2 presented methods are discussed in detail through a convergence analysis, followed by comparisons and verification using weighted residual methods on two beam-end loading cases (a slender straight beam and a slender circularly curved beam). Both in the convergence analysis and the two verification cases, BVP (7) is nondimensionalized for more general comparisons. Note that in the verification part, weighted residual methods are used as the standard since they have been proved to be an accurate and efficient method to solve (7) [15]. In the end, the proposed methods have been proved feasible and efficient to model CMs where three representative cases (two compliant parallelograms and one pre-buckled bistable mechanism) are studied with error analysis provided afterwards.

2. Solving large beam-deflection problems via Taylor series method and Padé approximant

2.1. Taylor series method

Taylor series is a simple and effective option to approximate a given analytic function within its radius of convergence [34]. Noticing the form of BVP (7), it's handy and straightforward to calculate derivatives at $s = 0$ considering the existence of trigonometric functions in the ODE along with one of the boundary conditions: $\theta(0) = 0$.

Therefore, we construct a Maclaurin series to approximate the solution of BVP (7):

$$\Theta(s) = \sum_{i=0}^{n} \frac{\frac{\mathrm{d}^i\theta}{\mathrm{d}s^i}(0)}{i!} s^i \tag{10}$$

where $\Theta(s)$ is noted as the approximate solution of (7) with order n and all $\frac{\mathrm{d}^i\theta}{\mathrm{d}s^i}(0)$ derivatives are obtained via using chain rule on the governing differential equation of (7) in an iterative manner (see the appendix for the detailed deduction).

As it has been shown in the appendix that any ith-order of $\frac{\mathrm{d}^i\theta}{\mathrm{d}s^i}(0)$ can be expressed as a function of one unknown variable $\frac{\mathrm{d}\theta}{\mathrm{d}s}(0)$, so for the sake of simplicity we note it as:

$$\frac{\mathrm{d}^i\theta}{\mathrm{d}s^i}(0) = f_i(\frac{\mathrm{d}\theta}{\mathrm{d}s}(0)) \tag{11}$$

where the functions f_i are given in the appendix. Consequently, we can arrive at the approximation of $\frac{\mathrm{d}\theta}{\mathrm{d}s}(s)$ expressed as a function of the unknown variable $\frac{\mathrm{d}\theta}{\mathrm{d}s}(0)$, i.e.,

$$\frac{\mathrm{d}\Theta}{\mathrm{d}s}(s) = \frac{\mathrm{d}(\sum_{i=0}^{n} \frac{\frac{\mathrm{d}^i\theta}{\mathrm{d}s^i}(0)}{i!} s^i)}{\mathrm{d}s} = \sum_{i=1}^{n} \frac{f_i(\frac{\mathrm{d}\theta}{\mathrm{d}s}(0))}{(i-1)!} s^{(i-1)} \tag{12}$$

Based on the above equation (12), 2 strategies can be adopted to implement Taylor series method to solve BVP (7) [35]:

1. "Explicit" strategy

   In this strategy, the second boundary condition provided in (7): $\frac{\mathrm{d}\theta}{\mathrm{d}s}(L) = \frac{M_o}{EI} + \frac{1}{R}$ is explicitly imposed, i.e.,

$$\frac{\mathrm{d}\Theta}{\mathrm{d}s}(L) = \sum_{i=1}^{n} \frac{f_i(\frac{\mathrm{d}\theta}{\mathrm{d}s}(0))}{(i-1)!} L^{(i-1)} = \frac{M_o}{EI} + \frac{1}{R} \tag{13}$$

which assumes that the series converges within $[0, L]$ if $n \to +\infty$. Logically, (12) will be a sufficient condition to numerically determine $\frac{\mathrm{d}\theta}{\mathrm{d}s}(0)$ when n is large enough. Besides, in (13) there is only one unknown: $\frac{\mathrm{d}\theta}{\mathrm{d}s}(0)$, and equivalently it is a low-dimensional model. Therefore, we can use Newton-Raphson method or other related methods to both directly and efficiently solve (13).

2. "Minimal" strategy
In this strategy, the auxiliary condition is obtained by imposing that the next or equivalently $(n+1)$th term of the truncated Taylor series vanishes, i.e.,

$$\frac{f_{n+1}(\frac{\mathrm{d}\theta}{\mathrm{d}s}(0))}{(n+1)!}L^{(n+1)} = 0 \tag{14}$$

where it is assumed that nth-order Maclaurin series converges within $[0, L]$, and then $n+1$th term possibly converges to 0, which is sufficient for numerically determining the value of $\frac{\mathrm{d}\theta}{\mathrm{d}s}(0)$. Obviously, we can solve this via Newton-Raphson method as well. Obviously, the complexity of (14) is less than that of (13).

Remark 3. *This "minimal" procedure is not always feasible to all types of functions in terms of Taylor expansion (Maclaurin expansion). For example, if we expand* $\sin(x)$ *using a Maclaurin series, we will have the following formulation:*

$$\sin(x) = x - \frac{x^3}{3!} + \frac{x^5}{5!} - \frac{x^7}{7!} + \frac{x^9}{9!}...$$

Then, we will always have:

$$\frac{\frac{\mathrm{d}^n(\sin(x))}{\mathrm{d}x^n}|_{x=0}}{n!}x^n = 0 \ \ (n = 2, 4, 6, 8, 10...)$$

Obviously, if the numerical solution of an ODE is $\sin(x)$ *within its corresponding domain, it's very likely to achieve some condition like (14) although the used Taylor series may not converge at all in its given domain.*

As long as the value of $\frac{\mathrm{d}\theta}{\mathrm{d}s}(0)$ is obtained using either of the above strategies, we can logically approximate $\theta(s)$ via (10).

2.2. Padé approximant (rational function method)

A Taylor series can often be accelerated quite dramatically (or turned from divergent to convergent) by being rearranged into a ratio of two such series. Supposing we have approximated the solution of BVP (7) using Maclaurin series shown in (10), we can then construct a rational function via:

$$\Theta(s) = \sum_{i=0}^{n} \frac{\frac{\mathrm{d}^i\theta}{\mathrm{d}s^i}(0)}{i!}s^i = \sum_{i=0}^{n} c_i s^i = \frac{P(s)}{Q(s)} = \frac{\sum_{i=0}^{p} a_i s^i}{\sum_{i=0}^{q} b_i s^i} \tag{15}$$

where $c_i = \frac{1}{i!}\frac{\mathrm{d}^i\theta}{\mathrm{d}s^i}(0)$, $P(s)$ and $Q(s)$ are polynomial functions of respective order p and q. (15) is called the Padé approximant $[p, q]$ of $\Theta(s)$. The unknown coefficients a_i and b_i of $P(s)$ and $Q(s)$ are determined by (10):

$$\begin{aligned} &P(s) = Q(s)\Theta(s) + o[s^{n+1}] \\ &Q(0) = 1 \\ &p + q = n \end{aligned} \tag{16}$$

equivalently,

$$c_0 + c_1 s + c_2 s^2 + ... = \frac{a_0 + a_1 s + a_2 s^2 + ...}{1 + b_1 s + b_2 s^2 + ...} \tag{17}$$

Multiplying up the denominator gives the following equivalent set of relations:

$$\begin{aligned} a_0 &= c_0 \\ a_1 &= c_1 + c_0 b_1 \\ a_2 &= c_2 + c_1 b_1 + c_0 b_2 \\ a_3 &= c_3 + c_2 b_1 + c_1 b_2 + c_0 b_3 \\ &... \end{aligned} \tag{18}$$

With c_i given (derived in Section. 2.1), each new line introduces 2 new unknowns, a_i and b_i. However, due to the constraint $p + q = n$, then there will be as many equations as unknowns (ignoring all terms $O(s^{p+q+1})$). For instance, if $n = 2$ and $p = q = 1$, then we have $a_0 = c_0$, $a_1 = c_1 + c_0 b_1$ and $0 = c_2 + c_1 b_1$
, i.e., 3 unknowns with 3 equations. Consequently, we can solve all these unknown coefficients a_i and b_i as functions of c_i, equivalently functions of $\frac{\mathrm{d}^i \theta}{\mathrm{d}s^i}(0)$.

Remark 4. *We need to take a look at the formulation of (15) first. In general, we have the following properties for rational functions:*

$$\begin{aligned} &\textit{if } p > q, \ \lim_{s\to+\infty} \Theta(s) = \lim_{s\to+\infty} \frac{\sum_{i=0}^{p} a_i s^i}{\sum_{i=0}^{q} b_i s^i} = +\infty \\ &\textit{if } p = q, \ \lim_{s\to+\infty} \Theta(s) = \lim_{s\to+\infty} \frac{\sum_{i=0}^{p} a_i s^i}{\sum_{i=0}^{q} b_i s^i} = \frac{a_p}{b_q} \\ &\textit{if } p < q, \ \lim_{s\to+\infty} \Theta(s) = \lim_{s\to+\infty} \frac{\sum_{i=0}^{p} a_i s^i}{\sum_{i=0}^{q} b_i s^i} = 0 \end{aligned}$$

*Obviously, $\Theta(s)$ will gradually converge to a fixed value $\frac{a_p}{b_q}$ (which is called the **horizontal asymptote** of the rational function) if $p = q$. Next, rearranging (1), (2), and (3), we can obtain:*

$$\frac{\mathrm{d}\theta}{\mathrm{d}s}(s) = \frac{F_y(x(L) - x(s)) + F_x(y(L) - y(s)) + M_o}{EI} + \frac{1}{R}$$

It is easy to notice that $\frac{\mathrm{d}\theta}{\mathrm{d}s}(s)$ will normally decrease and asymptotically reach $\frac{M_o}{EI} + \frac{1}{R}$ if $s \to L$. Therefore, $\theta(s)$, which is formulated as $\theta(s) = \int_0^s \frac{\mathrm{d}\theta}{\mathrm{d}s}(\xi)\mathrm{d}\xi$ will be logically bounded and also asymptotically reach a certain value as well if $s \to L$. Therefore, given the similar properties of both the physical phenomenon and rational functions, this paper sets $p = q = \frac{n}{2}$ where n is chosen to be even for Padé approximant.

Next, differentiating $\frac{P(s)}{Q(s)}$:

$$\frac{\mathrm{d}}{\mathrm{d}s}\left(\frac{P(s)}{Q(s)}\right) = \frac{P'(s)Q(s) - P(s)Q'(s)}{Q^2(s)} \tag{19}$$

and explicitly satisfying the second boundary condition $s = L$:

$$\frac{P'(L)Q(L) - P(L)Q'(L)}{Q^2(L)} = \frac{M_o}{EI} + \frac{1}{R} \tag{20}$$

where there is only one unknown $\frac{\mathrm{d}\theta}{\mathrm{d}s}(0)$, it can be therefore easily solved via Newton-Raphson method. Then, we can finalize the formulation of the rational function (15) to approximate the solution of (7):

$$\Theta(s) = \frac{\sum_{i=0}^{p} a_i s^i}{\sum_{i=0}^{q} b_i s^i} \tag{21}$$

Remark 5. *Considering the characteristics of rational functions, (21) may present the following* 2 *undesired properties in terms of characterizing or approximating* $\theta(s)$*:*

1. *if* $\sum_{i=0}^{q} b_i \tilde{s}^i = 0$ *and* $\sum_{i=0}^{p} a_i \tilde{s}^i = 0$*, (21) will have a hole at* $s = \tilde{s}$*.*
2. *if* $\sum_{i=0}^{q} b_i \tilde{s}^i = 0$ *and* $\sum_{i=0}^{p} a_i \tilde{s}^i \neq 0$*, (21) will have a vertical asymptote at* $s = \tilde{s}$*.*

Note that either of the above scenarios contracts the continuum hypothesis stated in solid mechanics. We can ignore the hole when numerically approximating $\theta(s)$ *in terms of the first. For the latter scenario, we need to change p and q (normally increase them) to avoid the vertical asymptote.*

2.3. Inflections points and nonlinear (post-)buckling

2.3.1. Inflections points along a deflected beam

According to [36] and [37], the essence of inflection points in a beam is all about the sign change of $\frac{\mathrm{d}\theta}{\mathrm{d}s}$. If no inflection point exists, the slope ($\frac{\mathrm{d}\theta}{\mathrm{d}s}$) is either monotonically increasing or decreasing, it must always be positive or negative, respectively. If an inflection point exists, the sign of $\frac{\mathrm{d}\theta}{\mathrm{d}s}$ changes once along the range of the independent variable $s \in [0, L]$. Mathematically speaking, if $\frac{\mathrm{d}\theta}{\mathrm{d}s}(s^*) = 0$ and $\frac{\mathrm{d}^2\theta}{\mathrm{d}s^2}(s^*) \neq 0$, then $s = s^*$ is an inflection point. For example, in nonlinear (post-)buckling of slender straight beams, inflection points are common (see Fig. 2a). The proposed methods numerically approximate the solution of BVP (7) so the inflection points will be implicitly treated by the proposed numerical methods while seeking the solution of BVP (7).

2.3.2. Nonlinear (post-)buckling

Note that there is a special type of beam-deflection scenarios called nonlinear buckling and post buckling. As shown in Fig. 2a, a slender straight beam fixed at one end is subjected to an axial force F_x. Its governing equation can be rearranged from BVP (7) as follows:

$$\begin{aligned} &\text{D.E.} \quad \frac{\mathrm{d}^2\theta}{\mathrm{d}s^2} = -\frac{F_y}{EI}(\cos\theta(s) + \frac{F_x}{F_y}\sin\theta(s)) = -\frac{F_x}{EI}\sin\theta(s) \\ &\text{B.C.} \quad \theta(0) = 0 \\ &\qquad \frac{\mathrm{d}\theta}{\mathrm{d}s}(L) = 0 \end{aligned} \tag{22}$$

Physically speaking, if F_x reaches the buckling limit, the straight slender beam will experience nonlinear buckling, possibly resulting in 3 different (deformed) beam shapes shown in Fig. 2a. For nonlinear post bucking of the studied slender beam, if we exert the same beam-end loading F_y and M_o after the slender beam buckles (for example, Geometry 1 and Geometry 3 in Fig. 2a), the slender beam will also end up with 2 possible equilibrium states (Geometry A and Geometry B in Fig. 2b). The corresponding governing BVP that describes the post buckling behavior of the slender beam can be formulated as:

$$\begin{aligned} &\text{D.E.} \quad \frac{\mathrm{d}^2\theta}{\mathrm{d}s^2} = -\frac{F_y}{EI}(\cos\theta(s) + \frac{F_x}{F_y}\sin\theta(s)) \\ &\text{B.C.} \quad \theta(0) = 0 \\ &\qquad \frac{\mathrm{d}\theta}{\mathrm{d}s}(L) = \frac{M_o}{EI} \end{aligned} \tag{23}$$

which is exactly the same as the original BVP (7).

Mathematically speaking, it is normal that BVPs may have multiple solutions given some specific conditions. Normally, in applied mathematics, the concept of bifurcation theory [38] needs to be introduced to solve these BVPs where some techniques are used, such as adjusting initial guesses, determining the boundary conditions by making most of the information of the governing equation, perturbation method and so on. For example, the proposed Taylor series method and Padé approximant can handle the 2 scenarios (buckling and post-buckling) via directly choosing the proper initial guess. This is quite handy than using weighted residual methods [15][39] since we only need to deal with just one initial guess of the unknown. Apparently, this specific topic is out of the scope of this paper, and will be further studied in our future work.

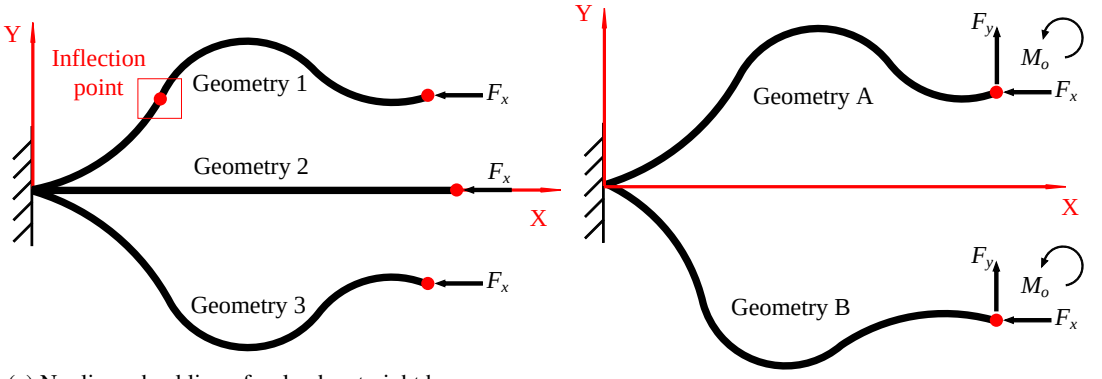

(a) Nonlinear buckling of a slender straight beam

(b) Nonlinear post buckling of a slender straight beam

Figure 2: Schematic graph of nonlinear buckling

2.4. Characterization of beam shape

Finally, we can characterize the deformed beam shape via:

$$x(s) = \int_0^s \cos(\Theta(\xi))\mathrm{d}\xi;\ y(s) = \int_0^s \sin(\Theta(\xi))\mathrm{d}\xi; \tag{24}$$

for $s \in [0, L]$ with L being the length of the deformed beam.

3. Convergence analysis and numerical validation

According to (7), it is obvious that modeling large deflection of slender beams is essentially a boundary value problem. In the first part of this section, we focus on the convergence analysis of Taylor series method and Padé approximant. Next, numerical testing is conducted to prove the feasibility of the used methods.

3.1. Prerequisites

In this paper, we first nondimensionalize the governing equation (7) for more general comparison. Therefore, the dependent variable θ and the independent variable s are nondimensionalized via:

$$\begin{aligned} \hat{\theta} &= \frac{\theta}{1};\ \theta = 1\hat{\theta} \\ \hat{s} &= \frac{s}{L};\ s = L\hat{s} \end{aligned} \tag{25}$$

Then, we can nondimensionalize (7) using (25) accordingly:

$$\frac{\mathrm{d}^2\hat{\theta}}{\mathrm{d}\hat{s}^2} = -\frac{F_y L^2}{EI}\cos\hat{\theta}(\hat{s}) - \frac{F_x L^2}{EI}\sin\hat{\theta}(\hat{s}) \tag{26}$$

with the corresponding nondimensionalized boundary conditions:

$$\begin{aligned} &\hat{\theta}(0) = 0 \\ &\frac{\mathrm{d}\hat{\theta}}{\mathrm{d}\hat{s}}(1) = \frac{M_o L}{EI} + \frac{L}{R} \end{aligned} \tag{27}$$

Reformulating (26) and (27), we can arrive at:

$$\begin{aligned} &\text{D.E.}\ \ \frac{\mathrm{d}^2\hat{\theta}}{\mathrm{d}\hat{s}^2} = -f_y\cos\hat{\theta}(\hat{s}) - f_x\sin\hat{\theta}(\hat{s}) \\ &\text{B.C.}\ \ \hat{\theta}(0) = 0 \\ &\qquad\ \ \frac{\mathrm{d}\hat{\theta}}{\mathrm{d}\hat{s}}(1) = m_o + \frac{1}{r} \end{aligned} \tag{28}$$

where

$$f_x = \frac{F_x L^2}{EI};\ f_y = \frac{F_y L^2}{EI};\ m_o = \frac{M_o L}{EI};\ r = \frac{R}{L};\ \hat{s} \in [0,1] \tag{29}$$

Logically, we will have the following:

$$\hat{x}(\hat{s}) = \int_0^{\hat{s}} \cos(\hat{\theta}(\xi))\mathrm{d}\xi;\ \hat{y}(\hat{s}) = \int_0^{\hat{s}} \sin(\hat{\theta}(\xi))\mathrm{d}\xi \tag{30}$$

where $\hat{x}(\hat{s})$ and $\hat{y}(\hat{s})$ are the nondimensionalized coordinates along the beam axis.

Remark 6. *It is noticed that ODE (28) essentially governs all sorts of large deflection problems under the framework of nondimensionalization where all physical parameters can be represented by nondimensionalized values (see (29) and (30)). This strategy provides both feasible and logical prerequisites for Section 3.2 and Section 3.3.*

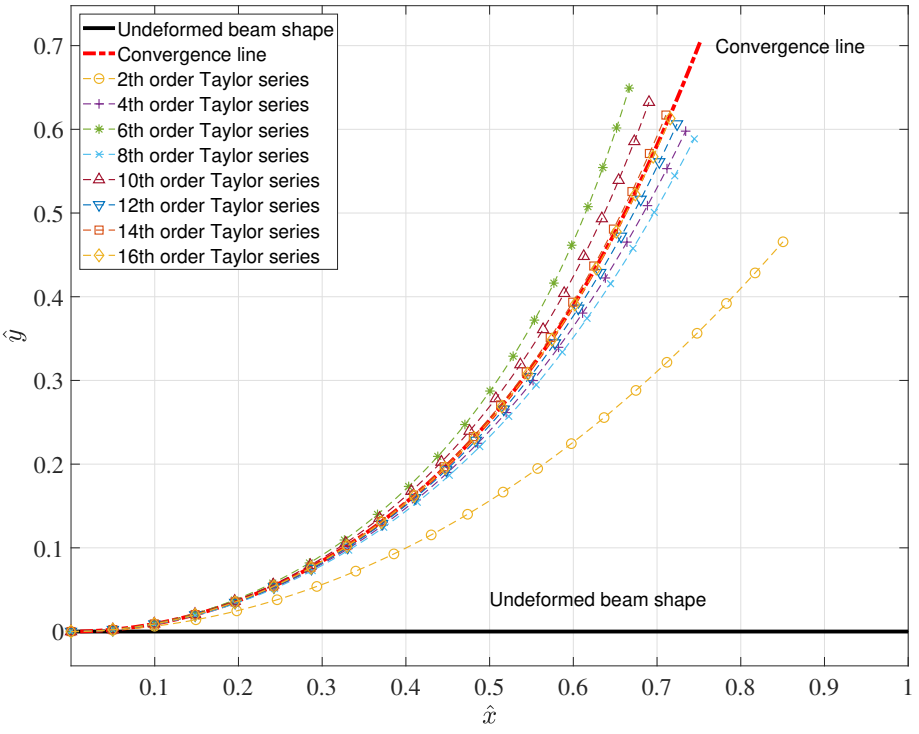

Figure 3: Convergence analysis on large-deflection problem of a slender straight beam using Taylor series

3.2. Convergence analysis

Mathematically speaking, we use a Taylor series or Padé approximant of limited order to approximate the solution of BVP (7). Obviously, it is not necessary to use a very high order since that may increase the complexity of numerical calculation. Moreover, a relatively low order may still present desired accuracy and convergence as well as high efficiency in its given domain. In general, we can implement an adaptive algorithm to determine the proper order of the Taylor series and Padé approximant: if $|\Theta_{n_k}(s) - \Theta_{n_{k-1}}(s)| \leq \epsilon$ where n_k is the kth option ($k = 1, 2, 3...$) for n and $\Theta_{n_k}(s)$ is the approximation using a polynomial of n_kth order, then n is settled: $n = n_k$; if not, $n = n_{k+1} = n_k + 1$. Likewise, a similar strategy can be implemented for Padé approximant as well.

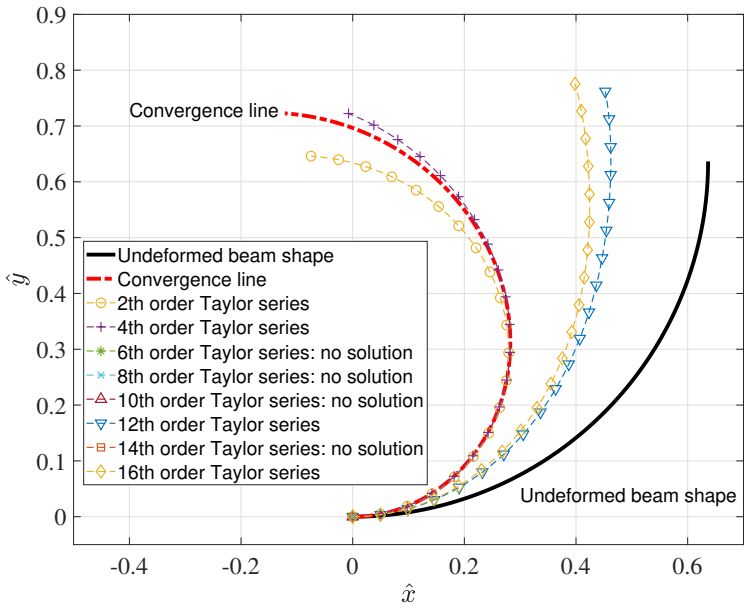

(a) Curvature-increasing deflection

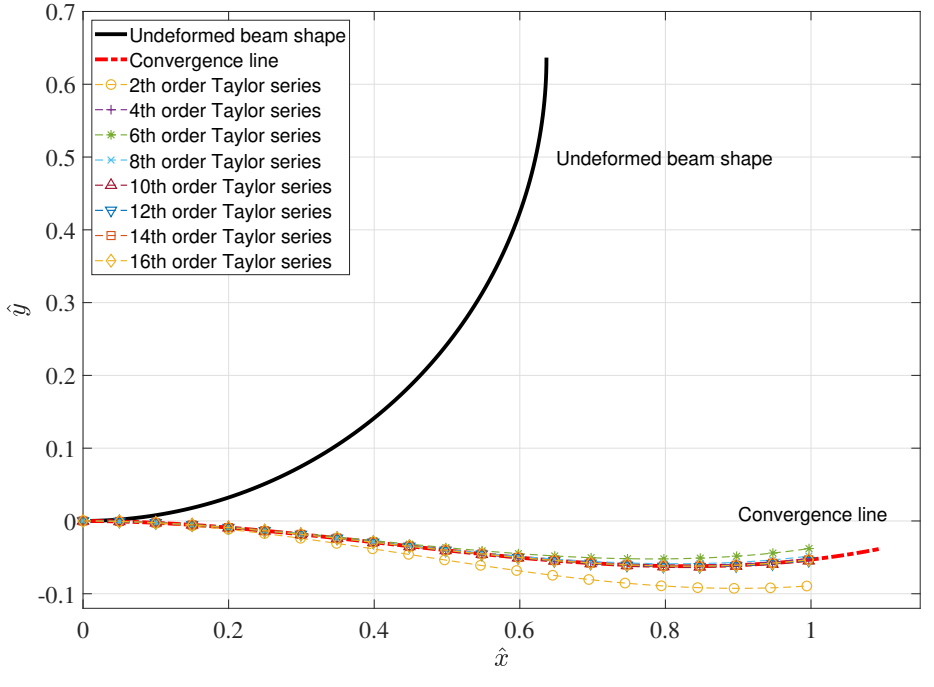

(b) Curvature-decreasing deflection

Figure 4: Convergence analysis on large-deflection problem of a slender circularly curved beam using Taylor series

However, as shown in [15], a polynomial with a well-chosen fixed order can already accurately approximate the solution of (7) in terms of modeling large deflection. Therefore, we are interested in determining the order of the feasible Taylor series or Padé approximant in advance to bypass the adaptive algorithm for more straightforward feasibility.

Besides, given the same order, Taylor series and Padé approximant may present different convergence properties (such as advantages and limitations) in terms of approximating the solution of BVP (7). Therefore, being aware of

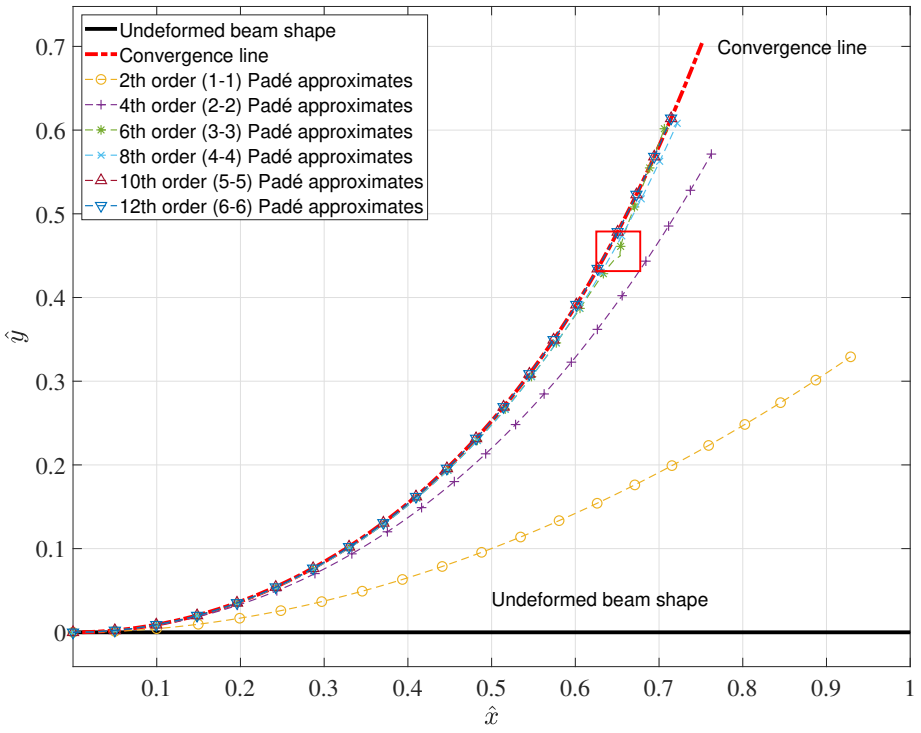

Figure 5: Convergence analysis on large-deflection problem of a slender straight beam using Padé approximant

these properties, we can choose the most suitable approximation methods for different targeted problems.

In this paper, we focus on the large deflections of slender straight beams and slender circularly curved beams under beam-end loading:

1. **Large deflection of a slender straight beam under beam-end loading**

$$f_x = 1.3;\ f_y = 0.8;\ m_o = 0.4;\ \frac{1}{r} = 0$$

2. **Large deflection of a slender circularly curved beam under beam-end loading**
   (a) **Curvature-increasing deflection**

$$f_x = 2.3;\ f_y = 1.5;\ m_o = 0.75;\ \frac{1}{r} = \frac{\pi}{2}$$

   (b) **Curvature-decreasing deflection**

$$f_x = -2.3;\ f_y = -1.5;\ m_o = -0.75;\ \frac{1}{r} = \frac{\pi}{2}$$

3.2.1. Taylor series method

As mentioned before, we are interested in setting up the proper order of the used Taylor series in terms of modeling large deflection problems. The deflections of a slender straight beam and a slender circularly curved beam are discussed respectively. The convergence of the series is of great importance in this method so the results of different orders will be analyzed in detail.

1. **Large deflection of a slender straight beam under beam-end loading:** in Fig. 3, as the order of the used Taylor series increases, the final deformed beam shape converges to a fixed curve (marked as **convergence**

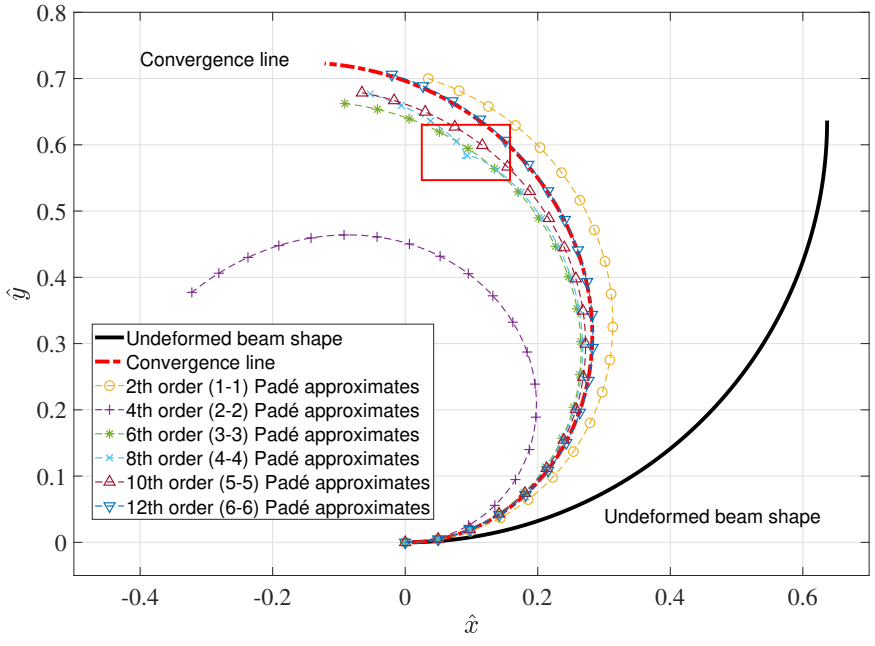

(a) Curvature-increasing deflection

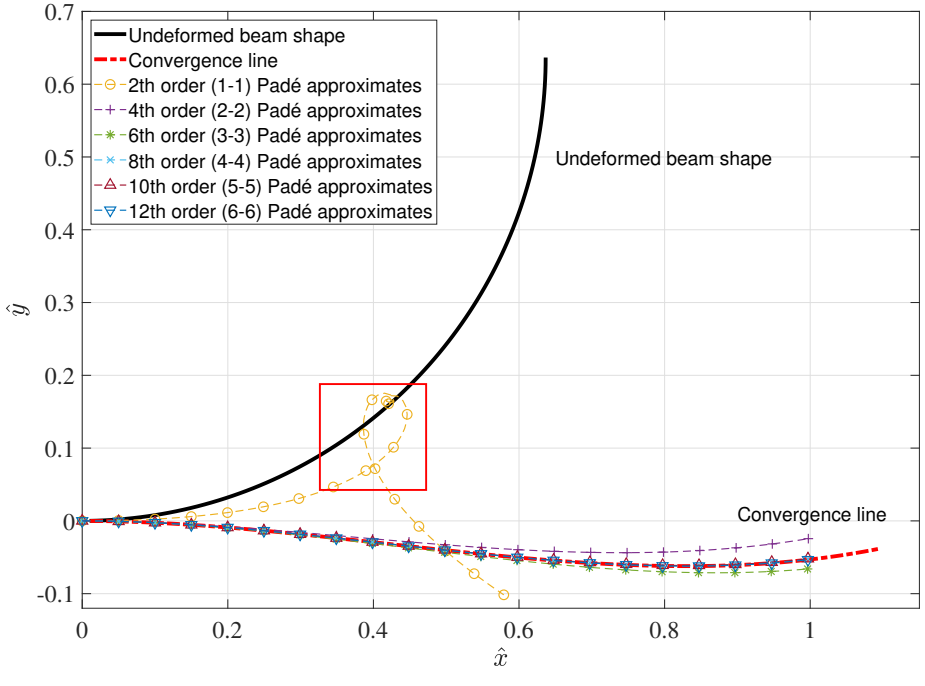

(b) Curvature-decreasing deflection

Figure 6: Convergence analysis on large-deflection problem of a slender circularly curved beam via Padé approximant

line) where in particular 14th-order series and 16th-order series almost cover each other and both converge to the convergence line. Generally speaking, a higher order of Taylor series normally can better approximate the original function within its radius of convergence [40]. However, for the studied problem, we have some extra constraints: two algebraic constraints represented by two boundary conditions and the ODE within the range $\hat{s} \in [0, 1]$. It is observed that in this case, the Taylor series subjected to the mentioned constraints turns out

to converge with gradually decreasing oscillation. And during this convergence, low order Taylor series may happen to present 'better' precision than high order one, as depicted in Fig. 3. The results imply that given a proper order, Taylor series method can converge in terms of solving BVP (28) in this case.

2. **Large deflection of a slender circularly curved beam under beam-end loading:**
   (a) **Curvature-increasing deflection:** in Fig. 4a, we cannot find solutions using 6th, 8th, 10th and 14th Taylor series even though the convergence criteria is set to be less restrictive. Moreover, the solutions found by the rest series do not present the trend of convergence at all when the order increases. Concluded from the results, Taylor series of even up to 16th order struggle to converge regarding solving BVP (7) of large anti-clockwise deflections of slender circularly curved beams.
   (b) **Curvature-decreasing deflection:** in Fig. 4b, on the contrary, Taylor series method presents great convergence in this case. The convergence trend of Taylor series is observed when the order increases, and series of orders up to 8th can converge to the convergence line well.

Remark 7. *It is observed that Taylor series present different convergence properties in terms of curvature-increasing and curvature-decreasing deflections. Mathematically speaking, the following are the possible reasons that make the Taylor series of a random function $f(x)$ fail to converge.*

(a) *If $f(x)$ is not infinitely differentiable, the Taylor series of $f(x)$ may not even be defined.*
(b) *If $f(x)$ is infinitely differentiable but not analytic,*
   i. *the derivatives of $f(x)$ at the expansion point may grow so quickly that the Taylor series may not converge. Equivalently, the radius of convergence is 0 in this case.*
   ii. *The series may converge to something other than $f(x)$.*
(c) *If $f(x)$ is analytic, its Taylor series about expansion point converges to the function in some neighborhood for every expansion point in its domain. However, the truncation error tends to grow rapidly away from expansion point if the order of the Taylor series is not large enough.*

In the case of curvature-increasing deflection, the constructed Taylor series expanded around $\hat{s} = 0$ struggles to converge. Due to the fact that $\hat{\theta}(\hat{s})$ increases more sharply (equivalently, the overall curvature gets larger within its domain) as independent variable $\hat{s}$ increases, it can be logically concluded that (b) and (c) could be the major contributing reasons. On the contrary, in the case of curvature-decreasing deflection, $\hat{\theta}(\hat{s})$ increases more slowly (equivalently, the overall curvature gets smaller within its domain) as independent variable $\hat{s}$ increases. Logically, the constructed Taylor series can more easily approximate the solution of BVP (7), which has been also numerically validated as shown in Fig. 4b.

3.2.2. Padé approximant

Likewise, choosing the proper order of the used Padé approximant is also of great importance. The deflections of a slender straight beam and a slender circularly curved beam are discussed in the following. The corresponding convergence analysis is provided.

1. **Large deflection of a slender straight beam under beam-end loading:** as shown in Fig. 5, Padé approximant of orders larger than 6th present great convergence in terms of approximating the solution of BVP (7). Padé approximant of 6th to 12th orders almost converges to the red dash line (convergence line) and cover each other closely. However, in particular, the curve of 6th Padé approximant has an abrupt change about $(0.65, 0.45)$ (the red box) in Fig. 5. This is due to the fact that in the form of the approximating rational function, there exists a vertical asymptote in its domain $\hat{s} \in [0, 1]$. See the detailed analysis in Remark 5. Overall speaking, Padé approximant of relatively low order can still present great convergence in this case.
2. **Large deflection of a slender circularly curved beam under beam-end loading:**
   (a) **Curvature-increasing deflection:** in Fig. 6a, it can be easily noticed that with the increase of the order, Padé approximant gradually converges to the red dash line (convergence line). With order up to 12th, its corresponding curve almost covers the convergence line. Therefore, we can draw the conclusion that it is feasible to achieve convergence using Padé approximant regarding solving BVP (7) of large deflections of slender circularly curved beams. In particular, the curve of 8th Padé approximant has an abrupt change about $(0.1, 0.59)$ (the red box) in Fig. 6a. The reason is explained in Remark 5.
   (b) **Curvature-decreasing deflection:** in Fig. 6b, Padé approximant gradually converges to the convergence line as the order increases. These rational functions of orders larger than 8th almost all cover the convergence line. In particular, the curve of 8th Padé approximant has an abrupt change about $(0.42, 0.12)$ (the red box) in Fig. 6b. The reason is explained in Remark 5.

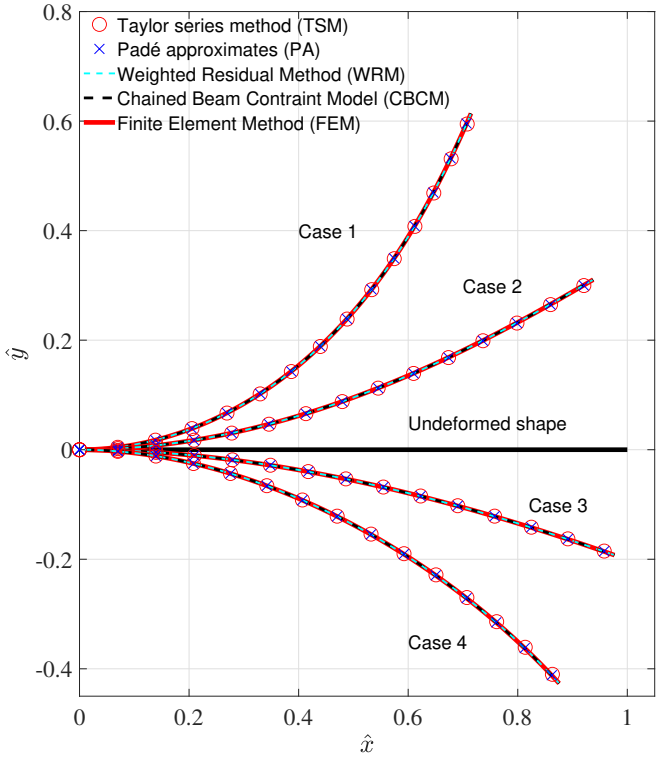

Figure 7: Comparison of graphical results of a deformed straight beam

	Case	Case 1	Case 2	Case 3	Case 4
Loading	f_x	1.3	0.65	−0.65	−2.6
	f_y	0.9	0.45	−0.45	−1.8
	m_o	0.4	0.2	−0.2	−0.8
TSM	$\hat{x}(1)$	0.7157	0.9379	0.9767	0.8769
	$\hat{y}(1)$	0.6130	0.3098	−0.1916	−0.4247
	$\hat{\theta}(1)$	1.1633	0.5324	−0.3357	−0.8255
	Order	16	8	4	16
PA	$\hat{x}(1)$	0.7145	0.9379	0.9767	0.8757
	$\hat{y}(1)$	0.6140	0.3098	−0.1918	−0.4264
	$\hat{\theta}(1)$	1.1663	0.5324	−0.3360	−0.8304
	Order	10	8	4	10
WRM	$\hat{x}(1)$	0.7146	0.9377	0.9765	0.8756
	$\hat{y}(1)$	0.6139	0.3104	−0.1924	−0.4266
	$\hat{\theta}(1)$	1.1658	0.5336	−0.3371	−0.8311
CBCM	$\hat{x}(1)$	0.7146	0.9376	0.9765	0.8756
	$\hat{y}(1)$	0.6139	0.3104	−0.1925	−0.4267
	$\hat{\theta}(1)$	1.1659	0.5336	−0.3372	−0.8311
	NOE	16	16	16	16
FEM	$\hat{x}(1)$	0.7149	0.9377	0.9766	0.8756
	$\hat{y}(1)$	0.6139	0.3104	−0.1925	−0.4269
	$\hat{\theta}(1)$	1.1657	0.5335	−0.3372	−0.8315
	NOE	15	15	15	15
ER_{TSM}	$\hat{x}(1)$	0.11%	0.02%	0.01%	0.15%
	$\hat{y}(1)$	0.15%	0.19%	0.47%	0.52%
	$\hat{\theta}(1)$	0.21%	0.21%	0.44%	0.08%
ER_{PA}	$\hat{x}(1)$	0.06%	0.02%	0.01%	0.01%
	$\hat{y}(1)$	0.02%	0.19%	0.36%	0.12%
	$\hat{\theta}(1)$	0.05%	0.21%	0.36%	0.08%
CE (s)	TSM	0.008	0.009	0.009	0.011
	PA	0.010	0.009	0.010	0.010
	WRM	0.020	0.027	0.012	0.017
	CBCM	0.20	0.30	0.25	0.35
	FEM	11	5	4	8

Table 1: Comparison of beam-end-coordinates of a deformed straight beam

3.2.3. Comparisons between the mentioned methods

Generally speaking, concluded from the above results, Padé approximant presents better convergence than the corresponding truncated Taylor series in terms of solving BVP (7). Specifically, Padé approximant performs well in both approximating the solution of the governing BVP for large deflection of straight beams and circularly curved beams even with a small number of series order. On the contrary, Taylor series method has been proved feasible only for analyzing large deflection of straight beams but with high-order series, and it struggles to converge in some cases of large deflection of circularly curved beams even under a high order. This is because Padé approximant makes most of the information of BVP (7) where the "shape" of the solution is pre-used by Padé approximant (the details are stated in Remark 4). However, Taylor series cannot be ensured to rapidly converge in all cases [35] where the details are stated in Remark 7. Compared to Taylor series method, Padé approximant has its unique limitations due to its formulation. As stated in Remark 5, the approximating rational functions might experience holes and vertical asymptotes in their domains, which contracts the continuum hypothesis of both solid mechanics and Euler Bernoulli beam theory. To handle this particular phenomenon, we can just increase the order of Padé approximant. From an engineering point of view, we choose TSM to analyze straight beams and PA to analyze circularly curved beams for further mechanism analysis.

3.3. Numerical validation

Based on the analysis stated in the last section, we then need to validate the proposed 2 methods through modeling a slender straight beam and a circularly curved beam under several beam-end loading scenarios where the deflected beam shapes and beam-end coordinates are studied. The graphical and numerical results are verified by beam-theory-based finite element method and compared by weighted residual method implemented in a global manner [15] and Chained Beam Constrained Model [18]. In the following of this section, FEM, CBCM, WRM, TSM and PA stand for finite element method, chained beam constrained model, weighted residual method, Taylor series method and Padé approximant respectively. Besides, ER, CE and NOE denote the error with respect to the results of FEM, computational expense and number of elements in FEM and CBCM.

3.3.1. A slender straight beam under beam-end loading:

Case 1: $f_x = 1.3;\ f_y = 0.9;\ m_o = 0.4;$
Case 2: $f_x = 0.65;\ f_y = 0.45;\ m_o = 0.2;$
Case 3: $f_x = -0.65;\ f_y = -0.45;\ m_o = -0.2;$
Case 4: $f_x = -2.6;\ f_y = -1.8;\ m_o = -0.8;$

As shown in Fig. 7, the deformed beam shapes under different beam-end loading are graphically presented. The graphical and coordinate results of TSM and PA have both been verified by FEM and compared by WRM and CBCM in Fig. 7 and Table 1. In particular, compared to TSM, PA of equal or even smaller order can still present slightly better results. TSM and PA are both slightly more time-saving than FEM, CBCM and WRM in terms computational expense (see Table 1).

3.3.2. A slender circularly curved beam under beam-end loading:

Case 1: $f_x = 2.3;\ f_y = 1.5;\ m_o = 0.75;\ \frac{1}{r} = \frac{\pi}{2}$
Case 2: $f_x = 0.69;\ f_y = 0.45;\ m_o = 0.225;\ \frac{1}{r} = \frac{\pi}{2}$
Case 3: $f_x = -0.69;\ f_y = -0.45;\ m_o = -0.225;\ \frac{1}{r} = \frac{\pi}{2}$
Case 4: $f_x = -2.3;\ f_y = -1.5;\ m_o = -0.75;\ \frac{1}{r} = \frac{\pi}{2}$

As shown in Fig. 8, the deformed beam shapes under different beam-end loading are graphically presented. The graphical and coordinate results of TSM and PA have both been verified by FEM and compared by CBCM and WRM in Fig. 8 and Table 2 where TSM is not used for analyzing curvature-increasing defection of the circularly curved beam due to the reasons stated in Remark 7. Similarly, compared to TSM, PA of equal or even smaller order can still present slightly better results. TSM and PA are both slightly more time-saving than FEM,CBCM and WRM in terms computational expense (see Table 2).

3.3.3. Discussions

Overall speaking, PA and TSM are both handy to deal with large deflection of slender beams (essentially solving BVP (7)) except that TSM struggles to handle curvature-increasing deflection of slender circularly curved beams (essentially struggling to approximate the solution of BVP (7) when its first-order derivative gets larger). It is interesting to notice that the rational functions generally present better accuracy than their truncated Taylor series in the case of solving BVP (7). However, the comparison between PA and TSM is still an ongoing subject in applied mathematics, and the convincing reasons as far as we can provide is stated in Remark 4. Besides, the less computational expense of TSM and PA is due to the fact that only one unknown is solved in these two methods where Newton-Raphson method only needs to deal with one-dimension Jacobin matrix (that is the slope of the function).

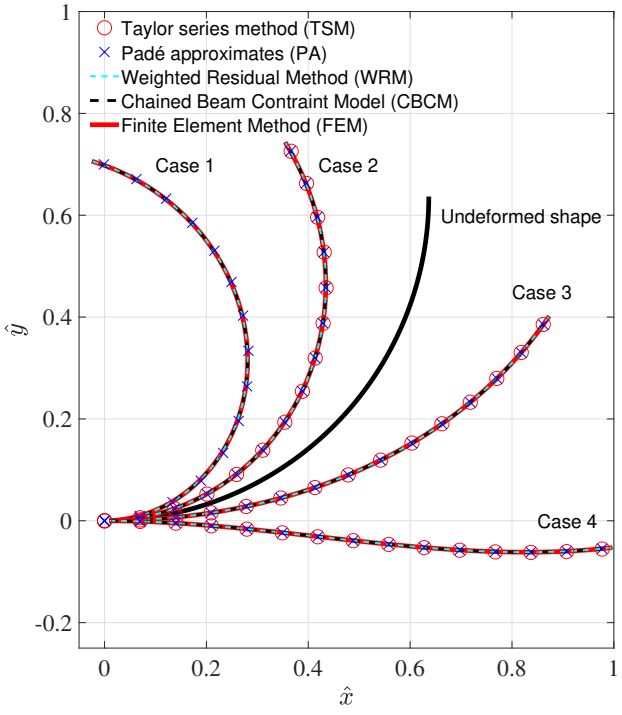

Figure 8: Comparison of graphical results of a deformed circularly-curved beam

	Case	Case 1	Case 2	Case 3	Case 4
Loading	f_x	2.3	0.69	−0.69	−2.3
	f_y	1.5	0.45	−0.45	−1.5
	m_o	0.75	0.225	−0.225	−0.75
TSM	$\hat{x}(1)$	NA	0.3564	0.8727	0.9969
	$\hat{y}(1)$	NA	0.7429	0.4020	−0.0534
	$\hat{\theta}(1)$	NA	2.1154	0.9779	0.1133
	Order	NA	16	8	14
PA	$\hat{x}(1)$	−0.0234	0.3549	0.8731	0.9969
	$\hat{y}(1)$	0.7062	0.7430	0.4015	−0.0526
	$\hat{\theta}(1)$	2.8426	2.1185	0.9766	0.1151
	Order	12	12	8	8
WRM	$\hat{x}(1)$	−0.0248	0.3546	0.8729	0.9969
	$\hat{y}(1)$	0.7060	0.7432	0.4018	−0.0527
	$\hat{\theta}(1)$	2.8522	2.1187	0.9775	0.1135
CBCM	$\hat{x}(1)$	−0.0232	0.3553	0.8726	0.9969
	$\hat{y}(1)$	0.7045	0.7430	0.4022	−0.0527
	$\hat{\theta}(1)$	2.8512	2.1180	0.9783	0.1148
	NOE	15	15	15	15
FEM	$\hat{x}(1)$	−0.0235	0.3549	0.8728	0.9969
	$\hat{y}(1)$	0.7044	0.7431	0.4019	−0.0527
	$\hat{\theta}(1)$	2.8523	2.1186	0.9776	0.1135
	NOE	24	24	24	24
ER_{TSM}	$\hat{x}(1)$	NA	0.42%	0.01%	0.00%
	$\hat{y}(1)$	NA	0.03%	0.02%	1.32%
	$\hat{\theta}(1)$	NA	0.15%	0.03%	0.18%
ER_{PA}	$\hat{x}(1)$	0.43%	0.08%	0.03%	0.00%
	$\hat{y}(1)$	0.26%	0.03%	0.10%	0.19%
	$\hat{\theta}(1)$	0.34%	0.01%	0.10%	1.41%
CE (s)	TSM	NA	0.04	0.05	0.05
	PA	0.06	0.04	0.02	0.02
	WRM	0.16	0.14	0.12	0.11
	CBCM	0.45	0.35	0.33	0.37
	FEM	17	8	9	19

Table 2: Comparison of beam-end-coordinates results of a deformed circularly-curved beam

4. Mechanisms synthesis using Taylor series method and Padé approximant

In this section, we aim to model 3 representative compliant mechanisms to prove the feasibility of Taylor series method and Padé approximant: straight-beam-based compliant parallelograms, circularly-curved-beam-based compliant parallelograms and mixed-type compliant parallelograms. These CMs are all of distributed compliance in their flexures. Not only verifying the feasibility of Taylor series method and Padé approximant for mechanism synthesis, we also aim to explore some desired characteristics of the aforementioned CMs for further optimization in our future work.

4.1. General methodology

For mechanism synthesis, we need to follow 3 modeling principles of mechanics [41][42][43]:

a) **Constitutive relationships**

b) **Force equilibrium or force compatibility relationships**

c) **Geometric equilibrium or geometric compatibility relationships**

These above 3 relationships govern the deformation of a flexible body. In other words, to model a CM, we need to develop the above three types of relationships, the corresponding equations of which need to be solved then through Newton-Raphson method. Finally, the modeling results are compared and verified by FEM results (where 3-D solid mesh element are used) with corresponding errors presented accordingly for further analysis.

4.2. Detailed modeling process and numerical results

4.2.1. Straight-beam-based compliant parallelogram

In this section, a straight-beam-based compliant parallelogram is modeled where Taylor series method is used to handle the constitutive beam equation, BVP (7). As demonstrated in Fig. 9, the compliant parallelogram consists of two slender straight beams parallel to each other (beam #1 and beam #2) and a rigid motion stage. Each of the slender beams is fixed at one end respectively (O_1 and O_2) and rigidly attached to a rigid motion stage on the other end. L, w and h refer to the length, width and thickness of the 2 involved elementary beams respectively. 2 local coordinate systems are set up for each flexible beam (see X_1-O_1-Y_1 and X_2-O_2-Y_2 in Fig. 9). The global coordinate frame X-O-Y is at the mid-point of O_1 and O_2. A combined load composed of F_K, P_K and M_K is exerted at the reference point K (the mid-point of AB), resulting in the deformed shape of the studied parallelogram mechanism shown in Fig. 9. F_A, P_A and M_A are the forces and moment applied at the tip A of beam #1 by the rigid motion stage. F_B, P_B and M_B are the forces and moment applied at the tip B of beam #2 by the rigid motion stage. Besides, A*, B* and K* refer to the corresponding points after deformation accordingly. Φ is the rotational angle of the motion stage. Note that $O_1O_2 = AB = T$ for this parallelogram mechanism.

1) **Constitutive relationships**

$$\begin{aligned} \textbf{Beam \#1:}\quad & \text{D.E.} \quad \frac{\mathrm{d}^2\theta_1}{\mathrm{d}s^2} = -\frac{F_A}{EI}(\cos\theta_1(s) + \frac{P_A}{F_A}\sin\theta_1(s)) \\ & \text{B.C.} \quad \theta_1(0) = 0 \\ & \qquad \frac{\mathrm{d}\theta_1}{\mathrm{d}s}(L) = \frac{M_A}{EI} \end{aligned} \tag{31}$$

$$\begin{aligned} \textbf{Beam \#2:}\quad & \text{D.E.} \quad \frac{\mathrm{d}^2\theta_2}{\mathrm{d}s^2} = -\frac{F_B}{EI}(\cos\theta_2(s) + \frac{P_B}{F_B}\sin\theta_2(s)) \\ & \text{B.C.} \quad \theta_2(0) = 0 \\ & \qquad \frac{\mathrm{d}\theta_2}{\mathrm{d}s}(L) = \frac{M_B}{EI} \end{aligned} \tag{32}$$

2) **Force equilibrium**

$$\begin{aligned} & F_K - F_A - F_B = 0;\ P_K - P_A - P_B = 0 \\ & M_K - M_A - M_B + F_K T/2\sin\Phi - P_K T/2\cos\Phi - F_B T\sin(\Phi) + P_B T\cos(\Phi) = 0 \end{aligned} \tag{33}$$

3) **Geometric compatibility relationships**

$$\begin{aligned} & \begin{bmatrix} x_A \\ y_A \end{bmatrix} = \begin{bmatrix} L \\ T/2 \end{bmatrix},\ \begin{bmatrix} x_{A^*} \\ y_{A^*} \end{bmatrix} = \begin{bmatrix} \int_0^L \cos\theta_1(s)\mathrm{d}s \\ \int_0^L \sin\theta_1(s)\mathrm{d}s \end{bmatrix} + \begin{bmatrix} 0 \\ T/2 \end{bmatrix} \\ & \begin{bmatrix} x_B \\ y_B \end{bmatrix} = \begin{bmatrix} L \\ -T/2 \end{bmatrix},\ \begin{bmatrix} x_{B^*} \\ y_{B^*} \end{bmatrix} = \begin{bmatrix} \int_0^L \cos\theta_2(s)\mathrm{d}s \\ \int_0^L \sin\theta_2(s)\mathrm{d}s \end{bmatrix} + \begin{bmatrix} 0 \\ -T/2 \end{bmatrix} \\ & \mathrm{AB} = [(x_A - x_B)^2 + (y_A - y_B)^2]^{0.5} = \mathrm{A^*B^*} = [(x_{A^*} - x_{B^*})^2 + (y_{A^*} - y_{B^*})^2]^{0.5} = T \\ & |x_{A^*} - x_{B^*}| = T\sin\Phi,\ \ |y_{A^*} - y_{B^*}| = T\cos\Phi,\ \ \theta_1(L) = \theta_2(L) = \Phi \\ & \begin{bmatrix} x_K \\ y_K \end{bmatrix} = \frac{1}{2}\begin{bmatrix} x_A \\ y_A \end{bmatrix} + \frac{1}{2}\begin{bmatrix} x_B \\ y_B \end{bmatrix},\ \begin{bmatrix} x_{K^*} \\ y_{K^*} \end{bmatrix} = \frac{1}{2}\begin{bmatrix} x_{A^*} \\ y_{A^*} \end{bmatrix} + \frac{1}{2}\begin{bmatrix} x_{B^*} \\ y_{B^*} \end{bmatrix},\ \begin{bmatrix} \Delta x \\ \Delta y \end{bmatrix} = \begin{bmatrix} x_{K^*} \\ y_{K^*} \end{bmatrix} - \begin{bmatrix} x_K \\ y_K \end{bmatrix} \end{aligned} \tag{34}$$

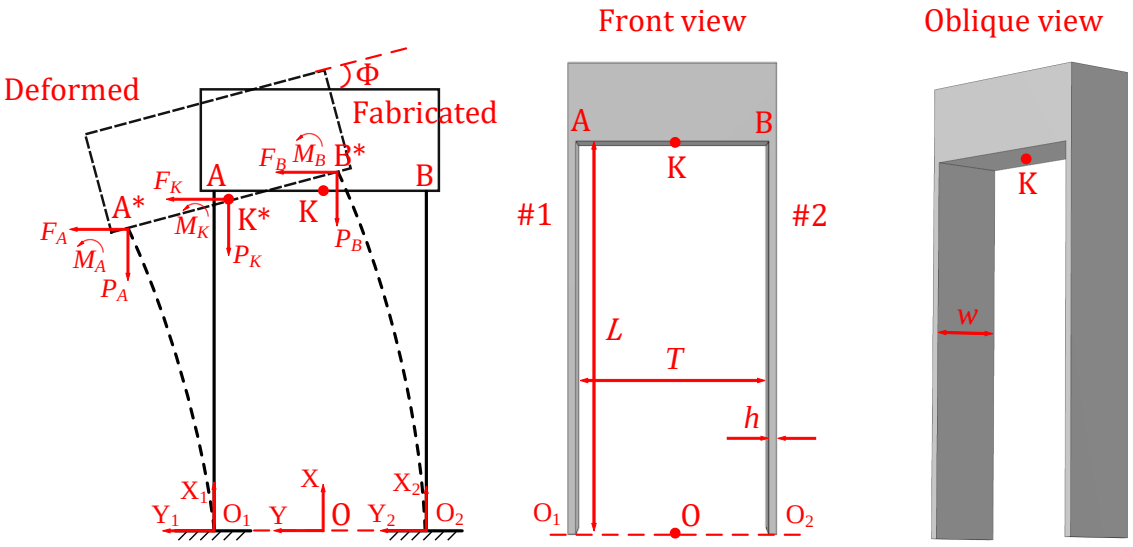

Figure 9: Constitutive, force equilibrium and compatibility relationships of a straight-beam-based compliant parallelogram and its schematic geometry

where $\begin{bmatrix} x_A & y_A \end{bmatrix}^T$, $\begin{bmatrix} x_{A^*} & y_{A^*} \end{bmatrix}^T$, $\begin{bmatrix} x_B & y_B \end{bmatrix}^T$, $\begin{bmatrix} x_{B^*} & y_{B^*} \end{bmatrix}^T$, $\begin{bmatrix} x_K & y_K \end{bmatrix}^T$ and $\begin{bmatrix} x_{K^*} & y_{K^*} \end{bmatrix}^T$ are the coordinates of A, A*, B, B*, K and K*. Then, we can numerically solve Eqs. (31) to (34) using Newton-Raphson method. Besides, $\begin{bmatrix} \Delta x & \Delta y & \Phi \end{bmatrix}^T$ refers to the translational and rotational displacements of K, the reference point of the modeled parallelogram mechanism. Modeling the studied revolute mechanism is all about the finding out the relationships between applied loads $\begin{bmatrix} F_K & P_K & M_K \end{bmatrix}^T$ and the corresponding displacements $\begin{bmatrix} \Delta x & \Delta y & \Phi \end{bmatrix}^T$ both at the reference point K. The material properties and geometry information are provided in the following:

$$E = 200 \times 10^9 \text{ Pa};\ w = 0.015 \text{ m};\ h = 0.0045 \text{ m};\ L = 0.25 \text{ m};\ I = \frac{wh^3}{12};\ T = 0 \text{ m}$$

Remark 8. *Note that $T = 0$ m is a special case of the studied parallelogram since the two slender straight beams cover each other in the plane of X-O-Y. Practically speaking, these two slender straight beams can be arranged normal to the screen as shown in Fig. 14a.*

The applied loads are set up as:

$$\begin{bmatrix} F_K \\ P_K \\ M_K \end{bmatrix} = iU = i \begin{bmatrix} 125 \text{ N} \\ 25 \text{ N} \\ 12.5 \text{ N.m} \end{bmatrix} \quad (i = 1, 2, 3, 4, \cdots, 10)$$

The results of iU and $\begin{bmatrix} \Delta x & \Delta y & \Phi \end{bmatrix}^T$ are provided via using the methodology stated in Section. 4.1 where the constitutive equations are solved by Taylor series method. These results are verified by solid-mechanics-based FEM verification (see Fig. 10). It is observed that Taylor series method presents high accuracy with errors (compared to FEM) all below 2%. In particular, the next-step initial guess is set up as the last-step answer for faster convergence [11]. The graphical results by FEM are shown in Fig. 14a where the fabricated and the $10U-$deformed mechanisms are graphically presented.

4.2.2. Circularly-curved-beam-based compliant parallelogram

In this section, a circularly-curved-beam-based compliant parallelogram is modeled where Padé approximant is used to handle the constitutive beam equation, BVP (7). As demonstrated in Fig. 11, the compliant parallelogram consists of two slender circularly-curved beams (beam #1 and beam #2) and a rigid motion stage. In particular, these two circularly-curved beams share the same center of circle. Each of the slender beams is fixed at one end respectively (O_1 and O_2) and rigidly attached to a rigid motion stage on the other end. Similarly, L, w and h refer

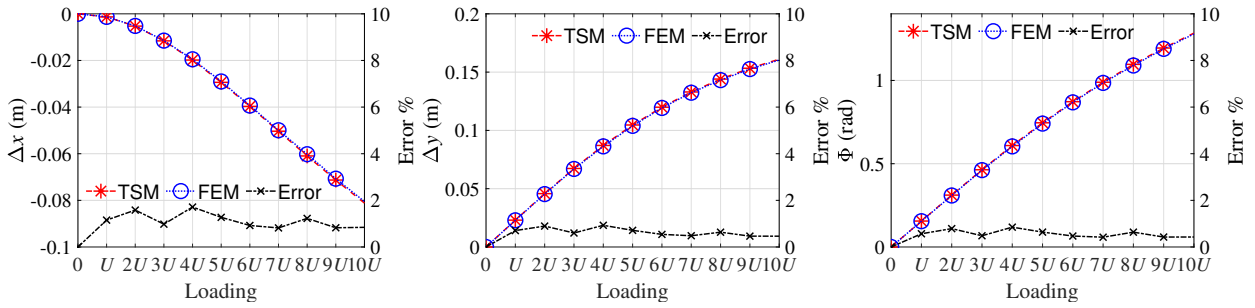

(a) $iU - \Delta x$ (b) $iU - \Delta y$ (c) $iU - \Phi$

Figure 10: Numerical results via Taylor series method

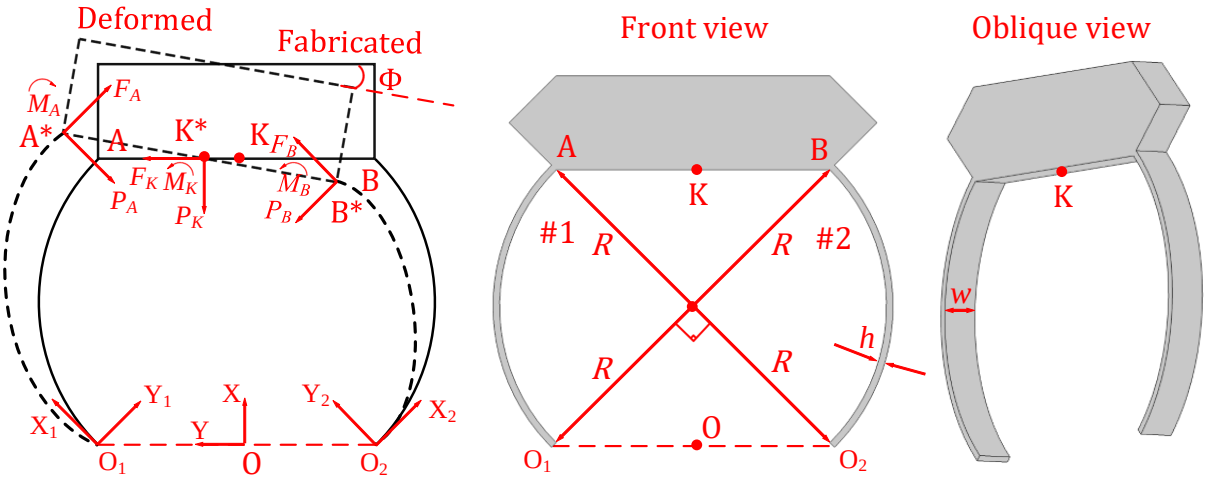

Figure 11: Constitutive, force equilibrium and compatibility relationships of a circularly-curved-beam-based compliant parallelogram and its schematic geometry

to the length, width and thickness of the 2 involved elementary beams respectively. 2 local coordinate systems are set up for each flexible beam (see X_1-O_1-Y_1 and X_2-O_2-Y_2 in Fig. 11). The global coordinate frame X-O-Y is at the mid-point of O_1 and O_2. A combined load composed of F_K, P_K and M_K is exerted at the reference point K (the mid-point of AB), resulting in the deformed shape of the studied parallelogram mechanism shown in Fig. 11. F_A, P_A and M_A are the forces and moment applied at the tip A of beam #1 by the rigid motion stage. F_B, P_B and M_B are the forces and moment applied at the tip B of beam #2 by the rigid motion stage. Besides, A*, B* and K* refer to the corresponding points after deformation accordingly. Φ is the rotational angle of the motion stage. Note that $O_1O_2 = T = 2R\sin(\angle O_2O_1B) = 2R\sin(\pi/4)$ due to the geometric relationship shown in Fig. 11.

1) **Constitutive relationships**

$$\textbf{Beam \#1:}\quad \text{D.E.}\quad \frac{\mathrm{d}^2\theta_1}{\mathrm{d}s^2} = -\frac{F_A}{EI}(\cos\theta_1(s) + \frac{P_A}{F_A}\sin\theta_1(s))$$
$$\text{B.C.}\quad \theta_1(0) = 0 \qquad (35)$$
$$\frac{\mathrm{d}\theta_1}{\mathrm{d}s}(L) = \frac{M_A}{EI} + \frac{1}{R}$$

$$\textbf{Beam \#2:}\quad \text{D.E.}\quad \frac{\mathrm{d}^2\theta_2}{\mathrm{d}s^2} = -\frac{F_B}{EI}(\cos\theta_2(s) + \frac{P_B}{F_B}\sin\theta_2(s))$$
$$\text{B.C.}\quad \theta_2(0) = 0 \tag{36}$$
$$\frac{\mathrm{d}\theta_2}{\mathrm{d}s}(L) = \frac{M_B}{EI} + \frac{1}{R}$$

$$\begin{aligned}
&F_K + P_A\cos(\frac{\pi}{4}) + F_A\cos(\frac{\pi}{4}) - P_B\cos(\frac{\pi}{4}) - F_B\cos(\frac{\pi}{4}) = 0\\
&P_K + F_A\sin(\frac{\pi}{4}) + F_B\sin(\frac{\pi}{4}) - P_A\sin(\frac{\pi}{4}) - P_B\sin(\frac{\pi}{4}) = 0\\
&M_K + M_A - M_B - F_K T/2\sin(\Phi) - P_K T/2\cos(\Phi) - F_B T\sin(\pi/4-\Phi) + P_B T\cos(\pi/4-\Phi) = 0
\end{aligned} \tag{37}$$

3) **Geometric compatibility relationships**

$$\begin{aligned}
&\begin{bmatrix}x_A\\y_A\end{bmatrix} = \begin{bmatrix}2R\sin(\pi/4)\\R\sin(\pi/4)\end{bmatrix},\ \begin{bmatrix}x_{A^*}\\y_{A^*}\end{bmatrix} = \begin{bmatrix}\cos\alpha & \sin\alpha\\-\sin\alpha & \cos\alpha\end{bmatrix}\begin{bmatrix}0 & 1\\1 & 0\end{bmatrix}\begin{bmatrix}\int_0^L\cos\theta_1(s)\mathrm{d}s\\\int_0^L\sin\theta_1(s)\mathrm{d}s\end{bmatrix} + \begin{bmatrix}0\\R\sin(\pi/4)\end{bmatrix}\\
&\begin{bmatrix}x_B\\y_B\end{bmatrix} = \begin{bmatrix}2R\sin(\pi/4)\\-R\sin(\pi/4)\end{bmatrix},\ \begin{bmatrix}x_{B^*}\\y_{B^*}\end{bmatrix} = \begin{bmatrix}\cos\alpha & \sin\alpha\\-\sin\alpha & \cos\alpha\end{bmatrix}\begin{bmatrix}\int_0^L\cos\theta_2(s)\mathrm{d}s\\\int_0^L\sin\theta_2(s)\mathrm{d}s\end{bmatrix} + \begin{bmatrix}0\\-R\sin(\pi/4)\end{bmatrix}\\
&\mathrm{AB} = [(x_A-x_B)^2+(y_A-y_B)^2]^{0.5} = \mathrm{A^*B^*} = [(x_{A^*}-x_{B^*})^2+(y_{A^*}-y_{B^*})^2]^{0.5} = T\\
&|x_{A^*}-x_{B^*}| = T\sin\Phi,\ \ |y_{A^*}-y_{B^*}| = T\cos\Phi,\ \ \theta_1(L)-\pi/2 = \pi/2-\theta_2(L) = \Phi\\
&\begin{bmatrix}x_K\\y_K\end{bmatrix} = \frac{1}{2}\begin{bmatrix}x_A\\y_A\end{bmatrix} + \frac{1}{2}\begin{bmatrix}x_B\\y_B\end{bmatrix},\ \begin{bmatrix}x_{K^*}\\y_{K^*}\end{bmatrix} = \frac{1}{2}\begin{bmatrix}x_{A^*}\\y_{A^*}\end{bmatrix} + \frac{1}{2}\begin{bmatrix}x_{B^*}\\y_{B^*}\end{bmatrix},\ \begin{bmatrix}\Delta x\\\Delta y\end{bmatrix} = \begin{bmatrix}x_{K^*}\\y_{K^*}\end{bmatrix} - \begin{bmatrix}x_K\\y_K\end{bmatrix}
\end{aligned} \tag{38}$$

where $\begin{bmatrix}x_A & y_A\end{bmatrix}^T$, $\begin{bmatrix}x_{A^*} & y_{A^*}\end{bmatrix}^T$, $\begin{bmatrix}x_B & y_B\end{bmatrix}^T$, $\begin{bmatrix}x_{B^*} & y_{B^*}\end{bmatrix}^T$, $\begin{bmatrix}x_K & y_K\end{bmatrix}^T$ and $\begin{bmatrix}x_{K^*} & y_{K^*}\end{bmatrix}^T$ are the coordinates of A, A*, B, B*, K and K*. Then, we can numerically solve Eqs. (31) to (34) using Newton-Raphson method. Besides, $\begin{bmatrix}\Delta x & \Delta y & \Phi\end{bmatrix}^T$ refers to the translational and rotational displacements of K, the reference point of the modeled parallelogram mechanism. Modeling the studied revolute mechanism is all about the finding out the relationships between applied loads $\begin{bmatrix}F_K & P_K & M_K\end{bmatrix}^T$ and the corresponding displacements $\begin{bmatrix}\Delta x & \Delta y & \Phi\end{bmatrix}^T$ both at the reference point K. The material properties and geometry information are provided in the following:

$$E = 200\times10^9\ \text{Pa};\ w = 0.015\ \text{m};\ h = 0.0045\ \text{m};\ L = 0.25\ \text{m};\ I = \frac{wh^3}{12};\ R = 2L/\pi;\ T = 2R\sin(\pi/4)$$

The applied loads are set up as:

$$\begin{bmatrix}F_K\\P_K\\M_K\end{bmatrix} = iU = i\begin{bmatrix}200\ \text{N}\\100\ \text{N}\\10\ \text{N.m}\end{bmatrix}\ (i = 1,2,3,4...9)$$

The results of iU and $\begin{bmatrix}\Delta x & \Delta y & \Phi\end{bmatrix}^T$ are provided via using the methodology stated in Section. 4.1 where the constitutive equations are solved by Padé approximant. These results are verified by solid-mechanics-based FEM (see Fig. 12). It is observed that Padé approximant presents high accuracy with maximum errors (compared to FEM) around 2%. Likewise, the next-step initial guess is set up as the last-step answer for faster convergence [11]. The graphical results by FEM are shown in Fig. 14b where the fabricated and the $9U-$deformed mechanisms are graphically presented.

Besides, the load-bearing ability is of great importance in terms of analyzing the performance of a compliant parallelogram. Here, we take the circularly-curved-beam-based compliant parallelogram for example to analyze its load-bearing ability via Padé approximant where the relationship between P_K and Δx is studied:

$$\begin{bmatrix}F_K\\P_K\\M_K\end{bmatrix} = iU = i\begin{bmatrix}0\ \text{N}\\100\ \text{N}\\0\ \text{N.m}\end{bmatrix}\ (i = -40,-39,\cdots,0,\cdots,39,40)$$

The numerical results are provided in Fig. 13 with the maximum errors (compared to FEM) around 3.5%.

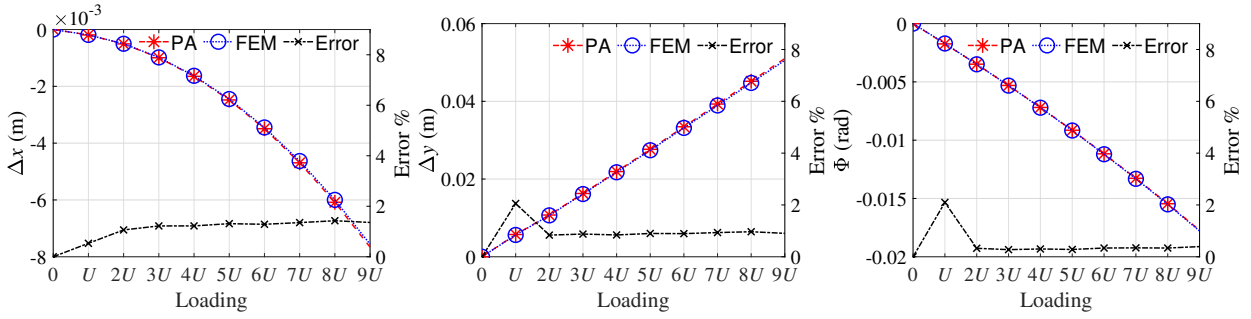

(a) $iU - \Delta x$ (b) $iU - \Delta y$ (c) $iU - \Phi$

Figure 12: Numerical results via Padé approximant

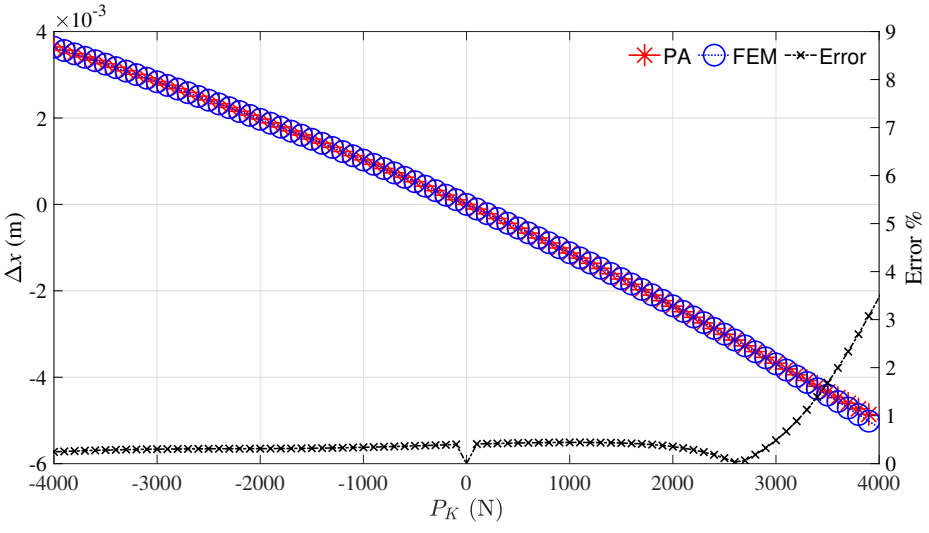

Figure 13: The relationship between P_K and Δx

4.2.3. Pre-bucked Bi-stable Mechanisms

Here, a special branch of CMs called Pre-bucked Bi-stable Mechanisms (PBM) [39] are modeled here to prove the feasibility of the proposed method in mechanism synthesis. As shown in Fig. 15, this PBM is composed of a slender straight beam fixed at one end and connected with a rigid passive joint. The translational and vertical motions of the beam end is realized by the cooperation of two rollers. The initiation of PBM is Scenario 1. As F_x is increased, the mechanism will end up with three possible states: still staying in Scenario 1; buckling into Scenarios 2 and 3. This special physical phenomena can be also described by Euler Bernoulli beam theory, which means we can use the proposed methods to handle the governing BVP. However, PBMs cannot be modeled through the normal procedure as presented in Section 2.2 since the existence of rigid joints in PBMs changes the governing equation of (7) and its boundary conditions. Therefore, we need to modify BVP (7) according to the practical constraints (see Fig. 15 and Fig. 16):

$$EI\frac{\mathrm{d}\theta}{\mathrm{d}s} = M(s) = F_x(y(L) - y(s)) \tag{39}$$

Then differentiating (39) leads to:

$$EI\frac{\mathrm{d}^2\theta}{\mathrm{d}s^2} = -F_x \sin\theta(s) \tag{40}$$

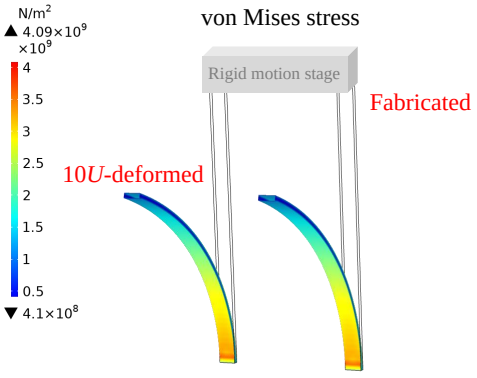

(a) The deflection of straight-beam-based compliant parallelogram

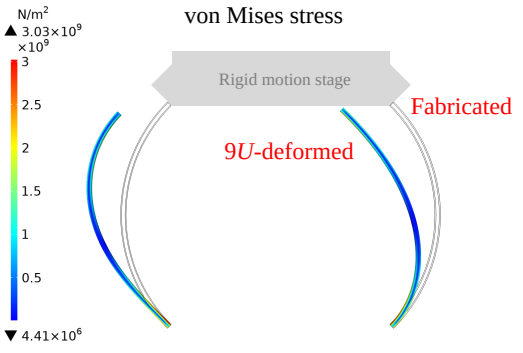

(b) The deflection of circularly-curved-beam-based compliant parallelogram

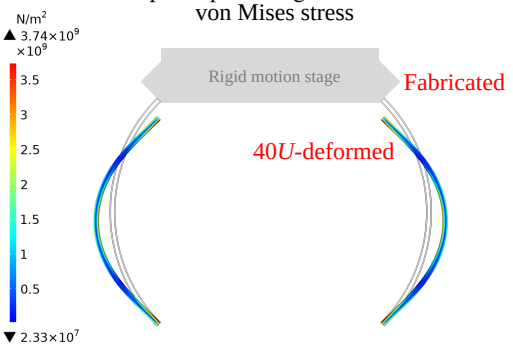

(c) The compression of circularly-curved-beam-based compliant parallelogram

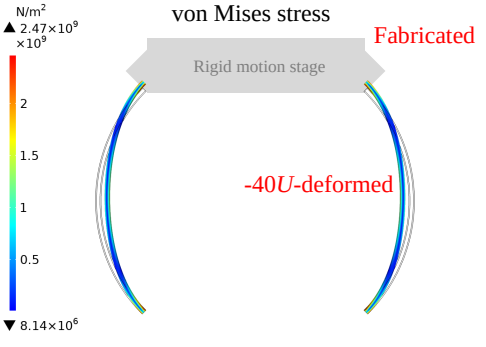

(d) The stretch of circularly-curved-beam-based compliant parallelogram

Figure 14: Graphical results evaluated by solid-mechanics-based Finite element method

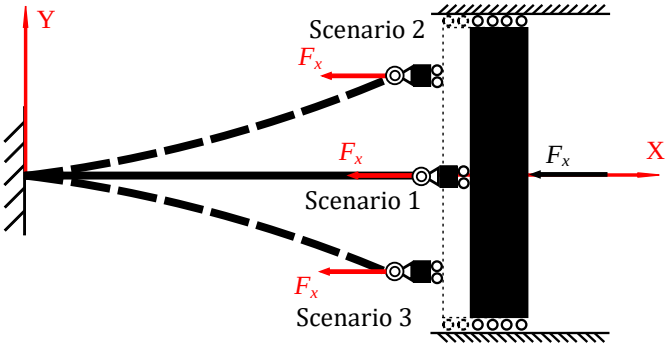

Figure 15: Schematic diagram of a Pre-bucked Bi-stable Mechanism

Rearranging (40), we will have the following:

$$\frac{1}{2}EI(\frac{\mathrm{d}\theta}{\mathrm{d}s})^2 - F_x\cos\theta(s) = C \tag{41}$$

where C is an unknown constant which can be determined by the boundary conditions. Precisely,

$$C = \frac{1}{2}EI(\frac{\mathrm{d}\theta}{\mathrm{d}s}(L))^2 - F_x\cos\theta(L) = -F_x\cos\alpha \tag{42}$$

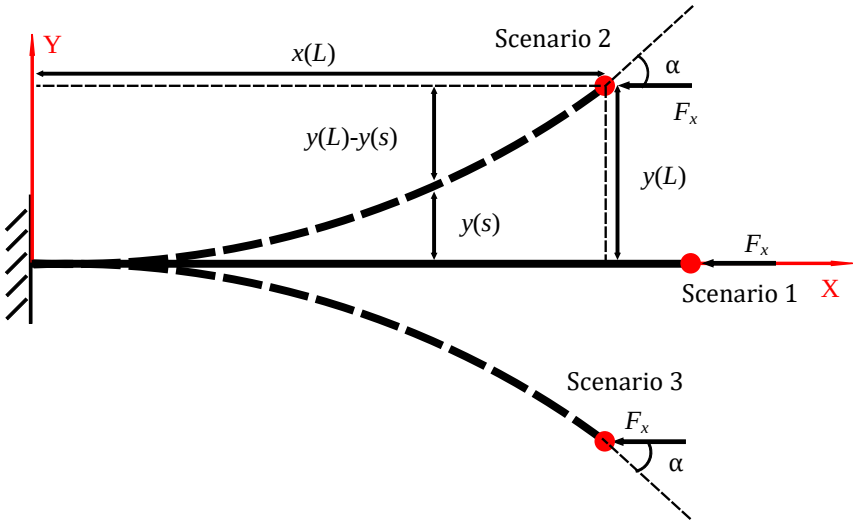

Figure 16: Detailed force diagram of the studied Pre-bucked Bi-stable Mechanism

where $EI\frac{\mathrm{d}\theta}{\mathrm{d}s}(L) = 0$ and $\theta(L) = \alpha$, and α is an unknown parameter to be determined. Similarly,

$$C = \frac{1}{2}EI(\frac{\mathrm{d}\theta}{\mathrm{d}s}(0))^2 - F_x\cos\theta(0) = \frac{F_x^2}{2EI}y(L)^2 - F_x \tag{43}$$

where $EI\frac{\mathrm{d}\theta}{\mathrm{d}s}(0) = F_x y(L)$ and $\theta(0) = 0$. Rearranging (42) drives us to have:

$$\frac{\mathrm{d}\theta}{\mathrm{d}s} = \pm\sqrt{\frac{2F_x}{EI}(\cos\theta(s) - \cos\alpha)} \tag{44}$$

which actually results in three possibilities. If $\theta(s) = 0$, then we can easily obtain $\alpha = \theta(s) = 0$ and $\frac{\mathrm{d}\theta}{\mathrm{d}s}(s) = 0$, which leads to Scenario 1 as shown in Fig. 16. Otherwise, we will have:

$$\frac{\mathrm{d}\theta}{\mathrm{d}s} = +\sqrt{\frac{2F_x}{EI}(\cos\theta(s) - \cos\alpha)} \tag{45}$$

if $\alpha > 0$ and

$$\frac{\mathrm{d}\theta}{\mathrm{d}s} = -\sqrt{\frac{2F_x}{EI}(\cos\theta(s) - \cos\alpha)} \tag{46}$$

if $\alpha < 0$, which clearly corresponds to Scenarios 2 and 3 as shown in Fig. 16. Here, we only take (45) for example to finish the rest deduction and logically solving (46) follows the same procedure. Assume $f(\alpha)$ as:

$$f(\alpha) = \int_0^{\alpha^-} \frac{1}{\sqrt{\frac{2F_x}{EI}(\cos\theta(s) - \cos\alpha)}}\mathrm{d}\theta - \int_{0^+}^{L^-}\mathrm{d}s \tag{47}$$

then we can obtain the value of α by solving $f(\alpha) = 0$ under Newton-Raphson method. So far, we have obtained all the information needed of the boundary conditions:

$$\text{B.C. } \theta(0) = 0,\ \theta(L) = \alpha,\ \frac{\mathrm{d}\theta}{\mathrm{d}s}(L) = 0 \tag{48}$$

As stated in Section 2.2, we can also define the approximate solution of (40):

$$\Theta(s) = \frac{P(s)}{Q(s)} \tag{49}$$

Therefore, we can arrive at the following relationships according to (48):

$$\begin{aligned} &\Theta(0) = 0 \\ &\Theta(L) = \alpha \\ &\frac{\mathrm{d}}{\mathrm{d}s}(\frac{P(s)}{Q(s)})|_{s=L} = \frac{P'(L)Q(L) - P(L)Q'(L)}{Q^2(L)} = 0 \end{aligned} \tag{50}$$

where similarly there is only one unknown $\frac{\mathrm{d}\theta}{\mathrm{d}s}(0)$ in the above equations. Then, we can use Newton's method to solve (50) directly. After obtaining the value of $\frac{\mathrm{d}\theta}{\mathrm{d}s}(0)$, we will be able to approximate the solution of (40) via (49). Then, we can calculate the coordinates of the beam end via:

$$x(L) = \int_0^L \cos(\Theta(s))\mathrm{d}s;\ y(L) = \int_0^L \sin(\Theta(s))\mathrm{d}s; \tag{51}$$

In this modeling, we are interested in how the external force F_x actuates the studied mechanism so the relationships of F_x-$x(L)$, F_x-$y(L)$ and F_x-α are studied (see Fig. 17). The material properties and geometry information are provided in the following:

$$E = 200 \times 10^9 \text{ Pa};\ w = 0.006 \text{ m};\ h = 0.001 \text{ m};\ L = 0.1 \text{ m};\ I = \frac{wh^3}{12}$$

4.3. Results analysis

4.3.1. Error analysis

Here, we aim to analyzing where the errors come from in the numerical models. According to Fig. 10, Fig. 12 and Fig. 13, Taylor series method and Padé approximant have proved effective in terms of mechanism synthesis (essentially dealing with the constitutive equations of slender straight beams and slender circularly-curved beams). Apart from the common numerical errors and model errors stated in [15], Taylor series method and Padé approximant have their unique numerical errors due to their intrinsic strategies of solving ODEs. Basically, both of them utilize the information of the studied ODE (where in this case BVP (7) is concerned) at one boundary to construct the approximate Taylor series or Padé approximant. Then, by satisfying another boundary, we will be able to find the proper series to approximate the solution to the studied ODE. However, in this process, the order of the used Taylor series or Padé approximant plays a rather important role. If it's not high enough, the solution will not converge to the correct answer (as shown in Fig. 3, Fig. 4, Fig. 5 and Fig. 6). Therefore, the numerical errors may also come from the improperly chosen order of the used Taylor series or Padé approximant. Logically, we can reduce these errors by increasing the order of the used Taylor series or Padé approximant.

4.3.2. Complexity of modeling

As we have stated in the appendix and according to (7), for a given order n, we can always deduce the analytic formulation of the nth derivative of θ at $s = 0$, and all those high-order derivatives are the functions of only one unknown variable $\frac{\mathrm{d}\theta}{\mathrm{d}s}(0)$. The whole modeling process tends to be complex due to the deductions of the final nonlinear equation to be solved. However, it is worth noting that those tedious deductions can be automatically obtained via symbolic computation software, such as Maple. For practical coding, Maple provides the interface to transform the formulation into the commonly used coding languages, like Matlab, Python, C sharp, fortran, java and so on for further mechanism synthesis. Therefore, the complexity of modeling via the proposed Taylor series method and Padé approximant could be logically deduced using proper mathematical tools.

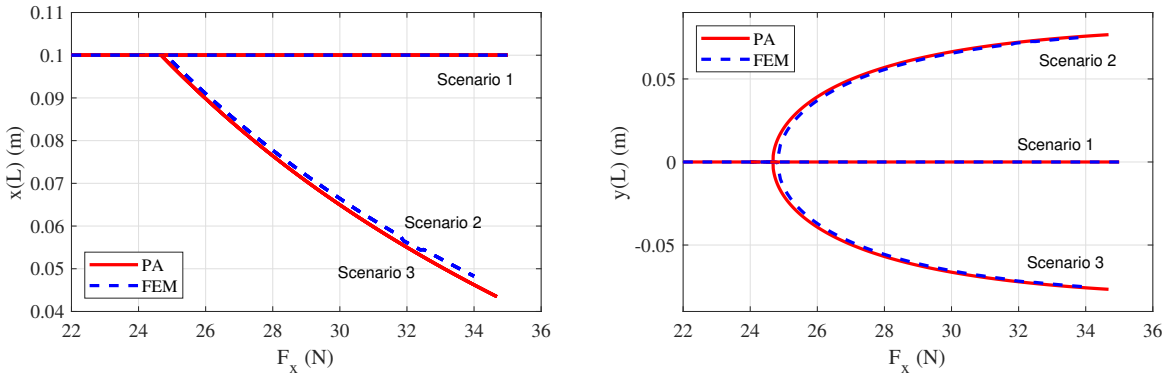

(a) F_x - $x(L)$ (b) F_x - $y(L)$

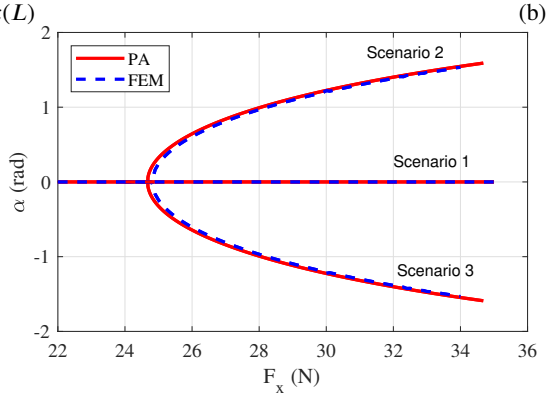

(c) F_x - α

Figure 17: Bifurcation diagrams of the studied PBM

5. Conclusions

Compliant mechanisms have been used as a promising option in many robotic systems where the built-in elementary flexible members play a dominant role in these mechanisms. Therefore, solving the constitutive equations of the elementary flexible members, such as slender straight beams and slender circularly-curved beams are a major focus. In this paper, we use Taylor series method and Padé approximant to solve the governing constitutive equations. Its accuracy and efficiency have been compared with weighted residual method and also verified by Finite Element Method (FEM) respectively. The feasibility of the proposed method has also been proved in terms of synthesizing CMs where three representative cases are studied. Our future work will focus on efficient numerical methods to solve the 3-D deflection of slender beams.

Declaration of Competing Interest

The authors declare that they have no known competing financial interests or personal relationships that could have appeared to influence the work reported in this paper.

Appendix: Iterative deduction of $\frac{\mathrm{d}^i\theta}{\mathrm{d}s^i}(0)$

According to the governing equation (7), we can easily obtain the 2nd-order derivative at 0 as:

$$\frac{\mathrm{d}^2\theta}{\mathrm{d}s^2}(0) = -\frac{F_y}{EI}(\cos\theta(0) + \frac{F_x}{F_y}\sin\theta(0)) = -\frac{F_y}{EI}$$

which in fact is constant.

Then, by differentiating (7) with respect to s and take the value $s = 0$, we can get the 3rd-order derivative at 0 as:

$$\frac{\mathrm{d}^3\theta}{\mathrm{d}s^3}(0) = -\frac{F_y}{EI}(-\sin\theta(0)\frac{\mathrm{d}\theta}{\mathrm{d}s}(0) + \frac{F_x}{F_y}\cos\theta(0)\frac{\mathrm{d}\theta}{\mathrm{d}s}(0)) = -\frac{F_x}{EI}\frac{\mathrm{d}\theta}{\mathrm{d}s}(0)$$

which indeed is a function of one unknown variable $\frac{\mathrm{d}\theta}{\mathrm{d}s}(0)$.

Calculating again the twice differentiation of (7) with respect to s and take $s = 0$, we obtain the 4th-order derivative at 0 as:

$$\begin{aligned}\frac{\mathrm{d}^4\theta}{\mathrm{d}s^4}(0) &= -\frac{F_y}{EI}(-\cos\theta(0)(\frac{\mathrm{d}\theta}{\mathrm{d}s}(0))^2 - \sin\theta(0)\frac{\mathrm{d}^2\theta}{\mathrm{d}s^2}(0) - \frac{F_x}{F_y}\sin\theta(0)(\frac{\mathrm{d}\theta}{\mathrm{d}s}(0))^2 + \frac{F_x}{F_y}\cos\theta(0)\frac{\mathrm{d}^2\theta}{\mathrm{d}s^2}(0)) \\ &= \frac{F_y}{EI}(\frac{\mathrm{d}\theta}{\mathrm{d}s}(0))^2 - \frac{F_x}{EI}\frac{\mathrm{d}^2\theta}{\mathrm{d}s^2}(0)\end{aligned}$$

which can be implicitly regarded as a function of one unknown variable $\frac{\mathrm{d}\theta}{\mathrm{d}s}(0)$, since it has been shown in the former calculation that $\frac{\mathrm{d}^2\theta}{\mathrm{d}s^2}(0)$ is a function of the unknown variable $\frac{\mathrm{d}\theta}{\mathrm{d}s}(0)$.

By iterating the above procedure, we can obtain the successive high-order derivatives $\frac{\mathrm{d}^i\theta}{\mathrm{d}s^i}(0)$, which gives the 5th-order derivative at 0 as:

$$\frac{\mathrm{d}^5\theta}{\mathrm{d}s^5}(0) = \frac{3F_y}{EI}\frac{\mathrm{d}^2\theta}{\mathrm{d}s^2}(0)\frac{\mathrm{d}\theta}{\mathrm{d}s}(0) - \frac{F_x}{EI}\frac{\mathrm{d}^3\theta}{\mathrm{d}s^3}(0) + \frac{F_x}{EI}(\frac{\mathrm{d}\theta}{\mathrm{d}s}(0))^3$$

the 6th-order derivative at 0 as:

$$\frac{\mathrm{d}^6\theta}{\mathrm{d}s^6}(0) = \frac{4F_y}{EI}\frac{\mathrm{d}^3\theta}{\mathrm{d}s^3}(0)\frac{\mathrm{d}\theta}{\mathrm{d}s}(0) + \frac{3F_y}{EI}(\frac{\mathrm{d}^2\theta}{\mathrm{d}s^2}(0))^2 - \frac{F_y}{EI}(\frac{\mathrm{d}\theta}{\mathrm{d}s}(0))^4 - \frac{F_x}{EI}\frac{\mathrm{d}^4\theta}{\mathrm{d}s^4}(0) + \frac{6F_x}{EI}\frac{\mathrm{d}^2\theta}{\mathrm{d}s^2}(0)(\frac{\mathrm{d}\theta}{\mathrm{d}s}(0))^2$$

the 7th-order derivative at 0 as:

$$\begin{aligned}\frac{\mathrm{d}^7\theta}{\mathrm{d}s^7}(0) = &\frac{5F_y}{EI}\frac{\mathrm{d}^4\theta}{\mathrm{d}s^4}(0)\frac{\mathrm{d}\theta}{\mathrm{d}s}(0) + \frac{10F_y}{EI}\frac{\mathrm{d}^3\theta}{\mathrm{d}s^3}(0)\frac{\mathrm{d}^2\theta}{\mathrm{d}s^2}(0) - \frac{10F_y}{EI}\frac{\mathrm{d}^2\theta}{\mathrm{d}s^2}(0)(\frac{\mathrm{d}\theta}{\mathrm{d}s}(0))^3 - \frac{F_x}{EI}\frac{\mathrm{d}^5\theta}{\mathrm{d}s^5}(0) + \frac{10F_x}{EI}\frac{\mathrm{d}^3\theta}{\mathrm{d}s^3}(0)(\frac{\mathrm{d}\theta}{\mathrm{d}s}(0))^2 \\ &+ \frac{15F_x}{EI}(\frac{\mathrm{d}^2\theta}{\mathrm{d}s^2}(0))^2\frac{\mathrm{d}\theta}{\mathrm{d}s}(0) - \frac{F_x}{EI}(\frac{\mathrm{d}\theta}{\mathrm{d}s}(0))^5\end{aligned}$$

the 8th-order derivative at 0 as:

$$\begin{aligned}\frac{\mathrm{d}^8\theta}{\mathrm{d}s^8}(0) = &\frac{15F_x}{EI}(\frac{\mathrm{d}^2\theta}{\mathrm{d}s^2}(0))^3 + \frac{6F_y}{EI}\frac{\mathrm{d}^5\theta}{\mathrm{d}s^5}(0)\frac{\mathrm{d}\theta}{\mathrm{d}s}(0) + \frac{15F_y}{EI}\frac{\mathrm{d}^4\theta}{\mathrm{d}s^4}(0)\frac{\mathrm{d}^2\theta}{\mathrm{d}s^2}(0) + \frac{10F_y}{EI}(\frac{\mathrm{d}^3\theta}{\mathrm{d}s^3}(0))^2 + \frac{F_y}{EI}(\frac{\mathrm{d}\theta}{\mathrm{d}s}(0))^6 \\ &+ \frac{15F_x}{EI}\frac{\mathrm{d}^4\theta}{\mathrm{d}s^4}(0)(\frac{\mathrm{d}\theta}{\mathrm{d}s}(0))^2 + \frac{60F_x}{EI}\frac{\mathrm{d}^3\theta}{\mathrm{d}s^3}(0)\frac{\mathrm{d}^2\theta}{\mathrm{d}s^2}(0)\frac{\mathrm{d}\theta}{\mathrm{d}s}(0) - \frac{15F_x}{EI}\frac{\mathrm{d}^2\theta}{\mathrm{d}s^2}(0)(\frac{\mathrm{d}\theta}{\mathrm{d}s}(0))^4 - \frac{20F_y}{EI}\frac{\mathrm{d}^3\theta}{\mathrm{d}s^3}(0)(\frac{\mathrm{d}\theta}{\mathrm{d}s}(0))^3 \\ &- \frac{45F_y}{EI}(\frac{\mathrm{d}^2\theta}{\mathrm{d}s^2}(0))^2(\frac{\mathrm{d}\theta}{\mathrm{d}s}(0))^2 - \frac{F_x}{EI}\frac{\mathrm{d}^6\theta}{\mathrm{d}s^6}(0)\end{aligned}$$

the 9th-order derivative at 0,

$$\begin{aligned}\frac{\mathrm{d}^9\theta}{\mathrm{d}s^9}(0) = &\frac{F_x}{EI}(\frac{\mathrm{d}\theta}{\mathrm{d}s}(0))^7 - \frac{F_x}{EI}\frac{\mathrm{d}^7\theta}{\mathrm{d}s^7}(0) - \frac{35F_y}{EI}\frac{\mathrm{d}^4\theta}{\mathrm{d}s^4}(0)(\frac{\mathrm{d}\theta}{\mathrm{d}s}(0))^3 + \frac{21F_y}{EI}\frac{\mathrm{d}^2\theta}{\mathrm{d}s^2}(0)(\frac{\mathrm{d}\theta}{\mathrm{d}s}(0))^5 + \frac{7F_y}{EI}\frac{\mathrm{d}^6\theta}{\mathrm{d}s^6}(0)\frac{\mathrm{d}\theta}{\mathrm{d}s}(0) \\ &+ \frac{21F_y}{EI}\frac{\mathrm{d}^5\theta}{\mathrm{d}s^5}(0)\frac{\mathrm{d}^2\theta}{\mathrm{d}s^2}(0) + \frac{35F_y}{EI}\frac{\mathrm{d}^4\theta}{\mathrm{d}s^4}(0)\frac{\mathrm{d}^3\theta}{\mathrm{d}s^3}(0) - \frac{105F_y}{EI}(\frac{\mathrm{d}^2\theta}{\mathrm{d}s^2}(0))^3\frac{\mathrm{d}\theta}{\mathrm{d}s}(0) + \frac{105F_x}{EI}(\frac{\mathrm{d}^2\theta}{\mathrm{d}s^2}(0))^2\frac{\mathrm{d}^3\theta}{\mathrm{d}s^3}(0) \\ &+ \frac{70F_x}{EI}(\frac{\mathrm{d}^3\theta}{\mathrm{d}s^3}(0))^2\frac{\mathrm{d}\theta}{\mathrm{d}s}(0) + \frac{21F_x}{EI}\frac{\mathrm{d}^5\theta}{\mathrm{d}s^5}(0)(\frac{\mathrm{d}\theta}{\mathrm{d}s}(0))^2 - \frac{35F_x}{EI}\frac{\mathrm{d}^3\theta}{\mathrm{d}s^3}(0)(\frac{\mathrm{d}\theta}{\mathrm{d}s}(0))^4 - \frac{105F_x}{EI}(\frac{\mathrm{d}^2\theta}{\mathrm{d}s^2}(0))^2(\frac{\mathrm{d}\theta}{\mathrm{d}s}(0))^3 \\ &+ \frac{105F_x}{EI}\frac{\mathrm{d}^4\theta}{\mathrm{d}s^4}(0)\frac{\mathrm{d}^2\theta}{\mathrm{d}s^2}(0)\frac{\mathrm{d}\theta}{\mathrm{d}s}(0) - \frac{210F_y}{EI}\frac{\mathrm{d}^3\theta}{\mathrm{d}s^3}(0)\frac{\mathrm{d}^2\theta}{\mathrm{d}s^2}(0)(\frac{\mathrm{d}\theta}{\mathrm{d}s}(0))^2\end{aligned}$$

the 10th-order derivative at 0 as:

$$\begin{aligned}\frac{\mathrm{d}^{10}\theta}{\mathrm{d}s^{10}}(0) = &\frac{168F_x}{EI}\frac{\mathrm{d}^5\theta}{\mathrm{d}s^5}(0)\frac{\mathrm{d}\theta}{\mathrm{d}s}(0)\frac{\mathrm{d}^2\theta}{\mathrm{d}s^2}(0) + \frac{280F_x}{EI}\frac{\mathrm{d}^4\theta}{\mathrm{d}s^4}(0)\frac{\mathrm{d}\theta}{\mathrm{d}s}(0)\frac{\mathrm{d}^3\theta}{\mathrm{d}s^3}(0) - \frac{560Fx}{EI}\frac{\mathrm{d}^3\theta}{\mathrm{d}s^3}(0)\frac{\mathrm{d}^2\theta}{\mathrm{d}s^2}(0)(\frac{\mathrm{d}\theta}{\mathrm{d}s}(0))^3\\
&- \frac{420F_y}{EI}\frac{\mathrm{d}^4\theta}{\mathrm{d}s^4}(0)\frac{\mathrm{d}^2\theta}{\mathrm{d}s^2}(0)(\frac{\mathrm{d}\theta}{\mathrm{d}s}(0))^2 - \frac{840F_y}{EI}(\frac{\mathrm{d}^2\theta}{\mathrm{d}s^2}(0))^2\frac{\mathrm{d}\theta}{\mathrm{d}s}(0)\frac{\mathrm{d}^3\theta}{\mathrm{d}s^3}(0) + \frac{28F_x}{EI}(\frac{\mathrm{d}\theta}{\mathrm{d}s}(0))^6\frac{\mathrm{d}^2\theta}{\mathrm{d}s^2}(0)\\
&+ \frac{280F_x}{EI}(\frac{\mathrm{d}^3\theta}{\mathrm{d}s^3}(0))^2\frac{\mathrm{d}^2\theta}{\mathrm{d}s^2}(0) + \frac{210F_x}{EI}\frac{\mathrm{d}^4\theta}{\mathrm{d}s^4}(0)(\frac{\mathrm{d}^2\theta}{\mathrm{d}s^2}(0))^2 - \frac{420F_x}{EI}(\frac{\mathrm{d}^2\theta}{\mathrm{d}s^2}(0))^3(\frac{\mathrm{d}\theta}{\mathrm{d}s}(0))^2 + \frac{8F_y}{EI}\frac{\mathrm{d}^7\theta}{\mathrm{d}s^7}(0)\frac{\mathrm{d}\theta}{\mathrm{d}s}(0)\\
&+ \frac{28F_y}{EI}\frac{\mathrm{d}^6\theta}{\mathrm{d}s^6}(0)\frac{\mathrm{d}^2\theta}{\mathrm{d}s^2}(0) + \frac{56F_y}{EI}\frac{\mathrm{d}^5\theta}{\mathrm{d}s^5}(0)\frac{\mathrm{d}^3\theta}{\mathrm{d}s^3}(0) - \frac{280F_y}{EI}(\frac{\mathrm{d}^3\theta}{\mathrm{d}s^3}(0))^2(\frac{\mathrm{d}\theta}{\mathrm{d}s}(0))^2 + \frac{56F_y}{EI}\frac{\mathrm{d}^3\theta}{\mathrm{d}s^3}(0)(\frac{\mathrm{d}\theta}{\mathrm{d}s}(0))^5\\
&+ \frac{210F_y}{EI}(\frac{\mathrm{d}^2\theta}{\mathrm{d}s^2}(0))^2(\frac{\mathrm{d}\theta}{\mathrm{d}s}(0))^4 + \frac{28F_x}{EI}\frac{\mathrm{d}^6\theta}{\mathrm{d}s^6}(0)(\frac{\mathrm{d}\theta}{\mathrm{d}s}(0))^2 - \frac{70F_x}{EI}\frac{\mathrm{d}^4\theta}{\mathrm{d}s^4}(0)(\frac{\mathrm{d}\theta}{\mathrm{d}s}(0))^4 - \frac{F_y}{EI}(\frac{\mathrm{d}\theta}{\mathrm{d}s}(0))^8\\
&- \frac{56F_y}{EI}\frac{\mathrm{d}^5\theta}{\mathrm{d}s^5}(0)(\frac{\mathrm{d}\theta}{\mathrm{d}s}(0))^3 + \frac{35F_y}{EI}(\frac{\mathrm{d}^4\theta}{\mathrm{d}s^4}(0))^2 - \frac{105F_y}{EI}(\frac{\mathrm{d}^2\theta}{\mathrm{d}s^2}(0))^4 - \frac{F_x}{EI}\frac{\mathrm{d}^8\theta}{\mathrm{d}s^8}(0)\end{aligned}$$

$$\frac{\mathrm{d}^{11}\theta}{\mathrm{d}s^{11}}(0) = ...$$

In summary, according to (7), for a given order n, we can always deduce the analytic formulation of the nth derivative of θ at $s = 0$, and all those high-order derivatives are the functions of only one unknown variable $\frac{\mathrm{d}\theta}{\mathrm{d}s}(0)$. It is worth noting that those tedious deductions can be automatically obtained via symbolic computation software, such as Mathematica and Maple.

References

[1] Larry L Howell. Compliant mechanisms. In 21st century kinematics. Springer, London, 2013.

[2] Nicolae Lobontiu. Compliant mechanisms: design of flexure hinges. CRC press, Boca Raton, 2020.

[3] D Farhadi Machekposhti, N Tolou, and JL Herder. A review on compliant joints and rigid-body constant velocity universal joints toward the design of compliant homokinetic couplings. Journal of Mechanical Design, 137(3), 2015.

[4] Shorya Awtar. Synthesis and analysis of parallel kinematic XY flexure mechanisms. PhD thesis, Massachusetts Institute of Technology, 2003.

[5] Sridhar Kota, Jinyong Joo, Zhe Li, Steven M Rodgers, and Jeff Sniegowski. Design of compliant mechanisms: applications to mems. Analog integrated circuits and signal processing, 29(1):7–15, 2001.

[6] Sridhar Kota, Joel A Hetrick, Russell Osborn, Donald Paul, Edmund Pendleton, Peter Flick, and Carl Tilmann. Design and application of compliant mechanisms for morphing aircraft structures. In Smart structures and materials 2003: industrial and commercial applications of smart structures technologies, volume 5054, pages 24–33. International Society for Optics and Photonics, 2003.

[7] Theodosia Lourdes Thomas, Venkatasubramanian Kalpathy Venkiteswaran, GK Ananthasuresh, and Sarthak Misra. Surgical applications of compliant mechanisms: A review. Journal of mechanisms and robotics, 13(2):020801, 2021.

[8] Jacob Greenwood, Alex Avila, Larry Howell, and Spencer Magleby. Conceptualizing stable states in origami-based devices using an energy visualization approach. Journal of Mechanical Design, 142(9):093302, 2020.

[9] Ke Wu and Gang Zheng. A comprehensive static modeling methodology via beam theory for compliant mechanisms. Mechanism and Machine Theory, 169:104598, 2022.

[10] Roland Bulirsch. Numerical calculation of elliptic integrals and elliptic functions. Numerische Mathematik, 7(1):78–90, 1965.

[11] Singiresu S Rao. The finite element method in engineering. Butterworth-heinemann, 2017.

[12] Mingxiang Ling, Larry L Howell, Junyi Cao, and Guimin Chen. Kinetostatic and dynamic modeling of flexure-based compliant mechanisms: a survey. Applied Mechanics Reviews, 72(3), 2020.

[13] Stefan Henning and Lena Zentner. Analysis of planar compliant mechanisms based on non-linear analytical modeling including shear and lateral contraction. Mechanism and Machine Theory, 164:104397, 2021.

[14] Stefan Henning, Sebastian Linß, Philipp Gräser, René Theska, and Lena Zentner. Non-linear analytical modeling of planar compliant mechanisms. Mechanism and Machine Theory, 155:104067, 2021.

[15] Ke Wu and Gang Zheng. Insight into numerical solutions of static large deflection of general planar beams for compliant mechanisms. Mechanism and Machine Theory, 169:104598, 2022.

[16] Shorya Awtar, Alexander H Slocum, and Edip Sevincer. Characteristics of beam-based flexure modules. Journal of Mechanical Design, 129(6), 2007.

[17] Guimin Chen and Fulei Ma. Kinetostatic modeling of fully compliant bistable mechanisms using timoshenko beam constraint model. Journal of Mechanical Design, 137(2), 2015.

[18] Fulei Ma and Guimin Chen. Modeling large planar deflections of flexible beams in compliant mechanisms using chained beam-constraint-model. Journal of Mechanisms and Robotics, 8(2), 2016.

[19] Yue-Qing Yu and Shun-Kun Zhu. 5r pseudo-rigid-body model for inflection beams in compliant mechanisms. Mechanism and Machine Theory, 116:501–512, 2017.

[20] Hai-Jun Su. A pseudorigid-body 3r model for determining large deflection of cantilever beams subject to tip loads. Journal of Mechanisms and Robotics, 1(2), 2009.

[21] Yue-Qing Yu, Zhong-Lei Feng, and Qi-Ping Xu. A pseudo-rigid-body 2r model of flexural beam in compliant mechanisms. Mechanism and Machine Theory, 55:18–33, 2012.

[22] Guimin Chen, Botao Xiong, and Xinbo Huang. Finding the optimal characteristic parameters for 3r pseudo-rigid-body model using an improved particle swarm optimizer. Precision Engineering, 35(3):505–511, 2011.

[23] Shun-Kun Zhu and Yue-Qing Yu. Pseudo-rigid-body model for the flexural beam with an inflection point in compliant mechanisms. Journal of Mechanisms and Robotics, 9(3), 2017.

[24] Yue-Qing Yu, Shun-Kun Zhu, Qi-Ping Xu, and Peng Zhou. A novel model of large deflection beams with combined end loads in compliant mechanisms. Precision Engineering, 43:395–405, 2016.

[25] Mohui Jin, Benliang Zhu, Jiasi Mo, Zhou Yang, Xianmin Zhang, and Larry L Howell. A cprbm-based method for large-deflection analysis of contact-aided compliant mechanisms considering beam-to-beam contacts. Mechanism and Machine Theory, 145:103700, 2020.

[26] Robert P Chase Jr, Robert H Todd, Larry L Howell, and Spencer P Magleby. A 3-d chain algorithm with pseudo-rigid-body model elements. Mechanics based design of structures and machines, 39(1):142–156, 2011.

[27] Venkatasubramanian Kalpathy Venkiteswaran and Hai-Jun Su. Pseudo-rigid-body models for circular beams under combined tip loads. Mechanism and Machine Theory, 106:80–93, 2016.

[28] Giuseppe Carleo, Ignacio Cirac, Kyle Cranmer, Laurent Daudet, Maria Schuld, Naftali Tishby, Leslie Vogt-Maranto, and Lenka Zdeborová. Machine learning and the physical sciences. Reviews of Modern Physics, 91(4):045002, 2019.

[29] Mohui Jin, Zhou Yang, Collin Ynchausti, Benliang Zhu, Xianmin Zhang, and Larry L Howell. Large-deflection analysis of general beams in contact-aided compliant mechanisms using chained pseudo-rigid-body model. Journal of Mechanisms and Robotics, 12(3), 2020.

[30] Carl T Kelley. Solving nonlinear equations with Newton's method. SIAM, 2003.

[31] Eugene Isaacson and Herbert Bishop Keller. Analysis of numerical methods. Courier Corporation, 2012.

[32] Hassaan Abbasi and Ali Javed. Implementation of differential transform method (dtm) for large deformation analysis of cantilever beam. In IOP Conference Series: Materials Science and Engineering, volume 899, page 012003. IOP Publishing, 2020.

[33] H Vázquez-Leal, Y Khan, AL Herrera-May, U Filobello-Nino, A Sarmiento-Reyes, V Manuel Jimenez-Fernandez, D Pereyra-Díaz, A Perez-Sesma, R Castaneda-Sheissa, A Díaz-Sanchez, et al. Approximations for large deflection of a cantilever beam under a terminal follower force and nonlinear pendulum. Mathematical Problems in Engineering, 2013, 2013.

[34] Murray R Spiegel. Advanced mathematics, volume 4. McGraw-Hill, Incorporated, 1991.

[35] Saeid Abbasbandy and C Bervillier. Analytic continuation of taylor series and the boundary value problems of some nonlinear ordinary differential equations. Applied Mathematics and Computation, 218(5):2178–2199, 2011.

[36] Chris Kimball and Lung-Wen Tsai. Modeling of flexural beams subjected to arbitrary end loads. J. Mech. Des., 124(2):223–235, 2002.

[37] Aimei Zhang and Guimin Chen. A comprehensive elliptic integral solution to the large deflection problems of thin beams in compliant mechanisms. Journal of Mechanisms and Robotics, 5(2), 2013.

[38] S-N Chow and Jack K Hale. Methods of bifurcation theory, volume 251. Springer Science & Business Media, 2012.

[39] Ke Wu and Gang Zheng. Theoretical analysis on nonlinear buckling, post-buckling of slender beams and bi-stable mechanisms. Journal of Mechanisms and Robotics, 14(3), 2022.

[40] Paul Dienes. The Taylor series: an introduction to the theory of functions of a complex variable. Dover New York, 1957.

[41] Jacob Pieter Den Hartog. Advanced strength of materials. Courier Corporation, 1987.

[42] Robert R Archer, Stephen H Crandall, Norman C Dahl, Thomas J Lardner, and M Srinivasan Sivakumar. An introduction to mechanics of solids. Tata McGraw-Hill Education, 2012.

[43] Stephen P Timoshenko and James N Goodier. Theory of elasticity. 1951.